

NASA Technical Memorandum 104739

IN-77

39708

P-62

TPS Design for Aerobraking at Earth and Mars

S. D. Williams
M. M. Gietzel
W. C. Rochelle
D. M. Curry

(NASA-TM-104739) TPS DESIGN FOR AEROPRAKING
AT EARTH AND MARS (NASA) 62 p CSCL 22B

N91-30970

Unclassified
G3/77 0039708

August 1991





TPS Design for Aerobraking at Earth and Mars

S. D. Williams, M. M. Gietzel, and W. C. Rochelle
Lockheed Engineering and Sciences Company
Houston, Texas

D. M. Curry
Lyndon B. Johnson Space Center
Houston, Texas

National Aeronautics and Space Administration
Lyndon B. Johnson Space Center
Houston, Texas

August 1991



Table of Contents

Summary	1
Introduction	1
Vehicle Configurations.....	3
Trajectory Definition	4
Aerodynamic Heating	6
TPS Materials	9
Structural Materials	10
TPS Sizing	10
Weight Analysis	13
Concluding Remarks	14
References	15

List of Tables

Table I	Basic Vehicle and Trajectory Design Parameters	19
Table II	Peak Heating Conditions for the Vehicles	20
Table III	Stagnation Point Heating and Pressure for the Vehicles Aerocapturing at Earth.	21
Table IV	Stagnation Point Heating and Pressure for the Vehicles Aerocapturing at Mars.....	25
Table V	Material Temperature Limits for TPS Materials	30
Table VI	Typical Benefits of Aerobraking.	31

List of Figures

Fig. 1	Sketch of the Vehicles Analyzed for Aerobraking at Mars and Earth.....	32
Fig. 2	Altitude vs. Time for the Earth Aerocapture Trajectories.....	33
Fig. 3	Velocity vs. Time for the Earth Aerocapture Trajectories.	33
Fig. 4	Pressure vs. Time for the Earth Aerocapture Trajectories.	34
Fig. 5	Altitude vs. Time for the Mars Aerocapture Trajectories.	34
Fig. 6	Velocity vs. Time for the Mars Aerocapture Trajectories.....	35
Fig. 7	Pressure vs. Time for the Mars Aerocapture Trajectories.....	35
Fig. 8	Convective Heating Rate for the Earth Aerocapture Trajectories.	36
Fig. 9	Radiative Heating Rate for the Earth Aerocapture Trajectories.....	36
Fig. 10	Combined Heating Rate for the Earth Aerocapture Trajectories.....	37
Fig. 11	Convective Heating Rate for the Mars Aerocapture Trajectories.....	37
Fig. 12	Radiative Heating Rate for the Mars Aerocapture Trajectories.	38
Fig. 13	Combined Heating Rate for the Mars Aerocapture Trajectories.	38
Fig. 14	Pressure Distributions for the Earth Aerocapture Vehicles.	39
Fig. 15	Heating Distributions for the Earth Aerocapture Vehicles.	39
Fig. 16	Pressure Distributions for the Mars Aerocapture Vehicles.....	40
Fig. 17	Heating Distributions for the Mars Aerocapture Vehicles.....	40
Fig. 18	Sketch of a Charring Ablator.	41
Fig. 19	Sketch of the Surface Energy Balance for a Charring Ablator.	41
Fig. 20	Sketch of the Reusable Thermal Models.	42
Fig. 21	Sketch of the Ablative Thermal Models.	43
Fig. 22	Radiation Equilibrium Temperature vs. S/L for Two Domed Cylinder Vehicles Entering at $\alpha = 55^\circ$ and 57°	44
Fig. 23	Mars Aerocapture for the 12.192 m AFE - Temperature Time History of Ablator Surface and Graphite Epoxy Backwall for the First 2000 Seconds at the Stagnation Point.	45
Fig. 24	Mars Aerocapture for the 12.192 m AFE - Predicted Ablation Rate at the Stagnation Point.	46
Fig. 25	Earth Aerocapture for the 12.192 m AFE - Temperature Time History of Ablator Surface and Graphite Epoxy Backwall for the First 2000 Seconds at the Stagnation Point.	47
Fig. 26	Earth Aerocapture for the 12.192 m AFE - 0.9 and 0.1 Char Density Ratio Depths at the Stagnation Point.	48
Fig. 27	Earth Aerocapture for the 12.192 m AFE - Predicted Ablation Rate at the Stagnation Point.	49
Fig. 28	TPS Unit Weight vs. Heat Load for a Vehicle (0.6096 m Biconic Entering at 8 km/s) Aerocapturing at Mars.	50
Fig. 29	TPS Unit Weight vs. Heat Load for a Vehicle (57° Domed Cylinder) Aerocapturing at Earth.	50
Fig. 30	Weight Penalty as a Function of Angle of Attack for Vehicles Aerocapturing at Earth.	51
Fig. 31	Weight Penalty as a Function of Entry Velocity for the Vehicles Aerocapturing at Mars.	51
Fig. 32	TPS Weight Penalty vs. Ballistic Coefficient for All Vehicles.....	52
Fig. 33	Weight Penalty Factors for Best TPS/Structure Weights.	52
Fig. 34	Weight Penalty Factors for Best TPS/Structure Weights with 20% Uncertainty...	53

Fig. 35	Percent Increase of GEO Delivery Mass for Aerobraked Stage Over an All Propulsive Stage.....	53
Fig. 36	Percent Increase in Payload Benefits for Aerobraking.....	54
Fig. 37	Relative Areas for the 57° Domed Cylinder TPS - Advanced Material Technology	55
Fig. 38	Relative Mass for the 57° Domed Cylinder TPS - Advanced Material Technology.	55
Fig. 39	Relative Areas for the 10 km/s Biconic TPS - Current Material Technology.....	55
Fig. 40	Relative Mass for the 10 km/s Biconic TPS - Current Material Technology.	55

TPS Design for Aerobraking at Earth and Mars

**S. D. Williams, M. M. Gietzel, W. C. Rochelle
Lockheed Engineering and Science Co., Houston, TX**

and

**D. M. Curry
Lyndon B. Johnson Space Center**

Summary

An investigation was made to determine the feasibility of using an aerobrake system for manned and unmanned missions to Mars, and to Earth from Mars and lunar orbits.

A preliminary Thermal Protection System (TPS) is examined for five unmanned small nose radius, straight biconic vehicles, and a scaled-up Aeroassisted Flight Experiment (AFE) vehicle aerocapturing at Mars. Analysis is also presented for the scaled-up AFE and an unmanned Sample Return Cannister (SRC) returning from Mars and aerocapturing into Earth orbit. Also analyzed were three different classes of Lunar Transfer Vehicles (LTVs): an expendable scaled-up modified Apollo Command Module (CM), a raked cone (modified AFE), and three large nose radius domed cylinders. The LTVs would be used to transport personnel and supplies between Earth and the Moon in order to establish a manned base on the lunar surface.

The TPS assessments for the Mars aerocapturing vehicles are made assuming either current material technology or advanced material using technology that should be available during the next decade. For the LTVs the TPS assessment is made assuming only advanced TPS material technology.

The TPS for all vehicles analyzed are shown to have an advantage over an all-propulsive velocity reduction for orbit insertion. Results indicate that TPS weight penalties of less than 28% can be achieved using current material technology for biconic vehicles entering Mars at 12 km/s or slower, but if advanced material technology is assumed, TPS weight penalties less than 23% can be achieved.

This study also indicates that a 12.2 m AFE aerocapturing at both Mars and Earth can be developed with a TPS weight penalty 50% less than that required for the small unmanned SRC using current material technology, and slightly less than the most favorable LTV using advanced material technology.

Introduction

Increased interest in the exploration of the solar system has been reflected in a renewed awareness for activities in space station planning, lunar base design, and related space exploration initiatives. In these preliminary design scenarios, it is assumed that the technology exists for transporting men from Earth to the Moon and back. However, due to the success of the Apollo and Shuttle Orbiter programs, the expectations for utilization of current technologies are greater today than in the past.

Two possible techniques can be used to place the vehicle in an initial parking orbit: propulsive burn and aerobraking. In an aerobraking system, a vehicle utilizes the planet's gravitational forces and atmosphere to reduce velocity, capture the vehicle, and place it into orbit. The aerobraking concept is intrinsically more desirable, from a conceptual viewpoint, than propulsive velocity reductions since this theoretically permits more vehicle weight to be used for payload instead of fuel. Roberts¹ found that a typical TPS plus structural weight to total vehicle weight ratio of 30% to 40% was favorable for aerobraking when considering weight tradeoffs for orbit transfers from Low Earth Orbit (LEO) to Geosynchronous Earth orbit (GEO). Roberts also indicated that from a practical viewpoint, due to the greater complexity posed by aerobraking, the tradeoff point is realistically more favorable at 20%, with 15% being even more desirable. For a round trip delivery from LEO to GEO or LEO to the lunar surface and back, similar results were obtained. For example, a 17% TPS weight penalty yields a 76% increase in payload over an all-propulsive stage for a lunar surface to LEO mission.

Current design scenarios call for establishing a base on the lunar surface and for developing a transportation system from the lunar orbit to Earth orbit prior to developing the transportation system to Mars. This analysis is directed towards aerobraking systems in which the vehicle is placed in a parking orbit about either Earth or Mars.

The TPS design requirements for manned spacecraft that enter Earth's atmosphere from a lunar orbit are more demanding than those required for the Space Shuttle Orbiter. This is due, in part, to the increased velocities required from vehicles entering from a lunar orbit instead of from LEO. Convective and radiative environments for vehicles entering the Earth's atmosphere have been extensively investigated. Lee and Goodrich,² for instance, compared pressure, convective, and radiative heating rate history data on the Apollo CM with wind tunnel data. Ried, Rochelle, and Milhoan developed the QRAD program³ to calculate radiation heating to blunt bodies entering the Earth's atmosphere.

A lesser number of investigations have been concerned with entry into planetary atmospheres having constituent gases differing from air. Of particular interest was an investigation in 1965 by Marvin and Deiwert⁴ that found the largest stagnation point heat transfer at constant flight velocity was obtained for argon, carbon dioxide, and air, respectively. Also of interest was a paper by Sutton and Graves⁵ in which they developed a general stagnation convective heating equation for arbitrary gas mixtures and found that heating in CO₂ was approximately 5% to 10% higher than for air. Sutton⁶ later developed a technique for calculating the radiation heating for a blunt body entering a CO₂ atmosphere.

Recent trajectory and simplified heating analyses for Mars entry and return missions have been performed by Tauber, Palmer, and Yang,⁷ and by Tauber, Bowles, and Yang.⁸ Other, more detailed flow-field and heating analyses for Mars entry and return have been reported by Park, Howe, Jaffe, and Candler,⁹ by Gupta, Sutton, Moss, and Lee,¹⁰ and by Carlson and Gally.¹¹

In all of the above studies, however, there was no vehicle TPS analysis performed. Williams, Pavlosky, and Curry¹² reported combined heating and TPS analysis for Mars-Earth entries. Henline¹³ subsequently reported a combined heating and TPS analysis for four separate ablators for a single vehicle. This analysis was only at the stagnation point, whereas in the work by Williams, et al., different vehicles and missions were considered with heating distributions, and a TPS sizing analysis was performed for each vehicle.

In the study by Williams, Pavlosky, and Curry,¹² it was shown that for the unmanned SRC returning from Mars it was necessary to use an ablator for aerocapturing in the Earth's atmo-

sphere. For this vehicle, a subscaled Apollo CM, the radiation equilibrium temperatures for a fully catalytic surface exceeded 2600°C. Using finite catalytic surface models, the radiation equilibrium temperatures for the LTV vehicles analyzed in this study were less than 2100°C for the moderate lift-to-drag ratio (L/D) vehicle ($m/C_L S = 409 \text{ kg/m}^2$), and less than 1700°C for the low L/D vehicle ($m/C_L S = 312 \text{ kg/m}^2$).

Five vehicles with three different configuration designs were analyzed to determine if aerobraking would be a viable alternative to an all-propulsive system for large man-rated vehicles returning from the moon. The LTVs included an expendable scaled-up Apollo CM, four reusable vehicles, a raked cone, and three large nose radius domed cylinders. The TPS for these vehicles was designed assuming advanced material technology that should be available by the end of the decade. One of the objectives was to assess whether a reusable TPS design could be developed for these vehicles in order to minimize repair and refurbishment costs. With the exception of the expendable vehicle, this objective can technically be achieved. Additionally, it was shown that the raked cone and the high angle-of-attack domed cylinder could achieve this objective with material technology development.

For the vehicles entering the Martian atmosphere, only the unmanned, low velocity, small nose radius, biconic vehicles do not require an ablative TPS. At higher velocities ablators will be required, but the advantage of aerobraking for velocity reduction and orbital insertion is retained.

The TPS for the 12.2 m AFE was analyzed using both advanced and current material technology. This vehicle, which aerocaptures at both Mars and Earth, can be developed with a TPS weight penalty that favors aerobraking. This provides a potential vehicle design that could be used to transport a crew and supplies between the Earth and Mars with an ablative TPS that requires refurbishment and maintenance after returning to Earth orbit.

This document will discuss in detail the vehicle configurations, trajectory definitions, and aerodynamic heating for aerobraking at Mars and Earth. TPS and structural materials used in the analyses associated with these missions are also presented. These results are then used to substantiate the payload benefits for both lunar return, Mars entry, and return aerobraking.

Vehicle Configurations

Three classes of LTVs are considered in this analysis: the moderate L/D domed cylinders (modified biconics), a low L/D raked-off right circular cone (modified AFE), and an expendable (scaled-up Apollo CM).^{14, 15} The two classes of vehicles that are being considered for entering the Martian atmosphere are the small nose radius biconics and the scaled up AFE.¹⁶ The scaled-up AFE and the SRC return from Mars to Earth. A sketch of these vehicles can be seen in figure 1.

The ground rules for the baseline LTVs used in this analysis stipulated construction would be on Earth (no on-orbit construction) and use a single stage compatible with a single launch lunar mission. These vehicles would be designed with a TPS using advanced TPS material technology, and use a composite material for the aeroshell structure. Advanced material TPS technology implies that this class of materials should be available within the next decade in opposition to the *current* material technology that is now available.

Similarly, for the unmanned Mars Rover Sample Return (MRSR) vehicles, it was stipulated that the vehicles be constructed on Earth and be dimensionally restricted such that they could be carried into Earth orbit in the Shuttle Orbiter payload bay. The TPS analyses for these vehicles

were based on both current and advanced material technology. Similar ground rules for the SRC and scaled-up AFE TPS and structure were assumed to be valid.

The physical characteristics for each vehicle are summarized in table I. The modified Apollo Command Module is a scaled-up version of the original CM designed to fit in the Orbiter payload bay. This vehicle is smaller than the other LTVs since it is expendable and jettisons all systems (including propulsion) not required to support the crew before entering the Earth's atmosphere. The design used in this analysis has a 4.37 m base diameter vehicle as opposed to the original CM's 3.91 m diameter.¹⁷

The raked cone vehicle (a modified AFE) is a raked-off right circular cone with low L/D. The cone half angle is 55° with a raked cut of 70°. This differs slightly from the AFE design which has an ellipsoid and an elliptical cone with circular cross sections in planes perpendicular to the cone axis.

The super-cargo-sized domed cylinder vehicle is 22.86 m long and 10.67 m in diameter, while the two smaller domed cylinder vehicles analyzed are 19.81m long and 8.53 m in diameter.

Two biconic vehicles considered in this analysis have a 0.30 m and a 0.61 m nose radius (R_N). The vehicles measure 9.91 m in total length with a 6.96 m aft conical section supporting a base diameter of 4.57 m and a 4° cone half angle. The 3.81 m forward section consists of the spherical nose cap attached to the conical section, which has cone half angle of either 23.55° or 20.69°, depending on the nose radius.

The AFE with the 12.2 m base diameter performs an aerocapture at Mars and returns to Earth, undergoing a second aerocapture maneuver. This vehicle is a scaled-up version of the original 4.27 m base diameter AFE. It was assumed to have an Earth entry weight of 13,151 kg, which is the same as determined from the work of Scott, et al.,¹⁸ for a 12.2 m AFE designed to enter from GEO.

The SRC is a subscaled Apollo CM with a base diameter of 1.8 m, and is carried to Mars in one of the biconics. The SRC returns to Earth for aerocapture after jettisoning its main propulsion system, retaining only the systems required for the specimen taken from the Martain surface.

For these vehicles, any reaction control systems and control surfaces were included as part of the vehicle weight at entry interface.

Trajectory Definition

Aerocapturing into orbit about a planetary object is a complex multifaceted problem involving uncertainties in the entry trajectory, planetary atmospheric modeling, and vehicle aerodynamic characteristics. Reference trajectories selected for aerocapture are designed to place the vehicles in a 500 km by 500 km orbit, both at Mars and at Earth. The characteristic parameters used to develop all trajectories can be seen in table I.

The LTV trajectories are designed to produce a maximum force of less than 5 Gs on the crew. The altitude profiles for these vehicles can be seen in figure 2, and the velocity profiles are presented in figure 3. From these figures it is clear that the Apollo CM penetrates deeper into the atmosphere (59.5 km) than the other LTVs, and the raked cone enters shallower (70.6 km) and remains longer in the atmosphere. The behavior of the three domed cylinders was fairly

similar with a maximum altitude variation of 4 km, from 64.6 km for the vehicle entering at 40° to 68.2 km for the vehicle entering at 57°. The stagnation pressure profiles for these vehicles can be seen in figure 4.

An L/D of 1.0 for the biconic vehicles provides the control authority required for the aeropass maneuver. The trajectories for these vehicles were analyzed in a previous study, entering the Martian atmosphere at 5.89 km/s and 7.81 km/s with a constant angle of attack (α) of 27° and 20°, respectively. The low velocity trajectory was rerun using a slightly lower velocity (5.88 km/s), but with the same flight path angle and angle of attack. The two new trajectories have higher entry velocities of 9.75 km/s and 11.76 km/s and are defined for a vehicle entering at $\alpha = 20^\circ$, the same as used for the 8 km/s trajectory.

The 0.3 m R_N vehicle was analyzed only for the 6 km/s trajectory, with respect to heating and TPS assessments, while the 0.61 m R_N vehicle was analyzed for all four trajectories (6, 8, 10, and 12 km/s). Figures 5, 6, and 7 show the altitude, velocity, and stagnation pressure as a function of time for these trajectories. In general, the higher the initial velocity the deeper the penetration into the atmosphere and the longer the vehicle remains in the atmosphere before exiting to orbital flight conditions.

Similar to the domed cylinder LTVs, the biconics had a variation of 4 km over the 6 km/s velocity range. A minimum altitude of 42.1 km was attained by the vehicle entering at 12 km/s in comparison to the 46.5 km altitude attained by the 6 km/s biconic. In comparison with the lower L/D LTVs, the biconics remain in the atmosphere approximately twice as long and penetrate deeper into the atmosphere.

The 12.2 m modified AFE enters Mars' atmosphere at the moderate 8 km/s velocity similar to that for the MRSR biconic vehicle, except that this vehicle enters at $\alpha = 0^\circ$ (natural trim of 17°) instead of the 20° used for the biconic. The AFE trajectories are designed to produce a maximum force of less than 5 Gs on the crew.

The flight path angles were fairly similar for all vehicles aerocapturing at Mars. Figures 5, 6, and 7 also show the altitude, velocity, and pressure as a function of time for the Mars trajectory, while figures 2, 3, and 4 provide the same information for the return to Earth. With its low L/D, the AFE does not provide the same control authority during the aeropass maneuver as is afforded the biconics. At this time this vehicle would not be considered for a Mars aerocapture due to this lack of control authority; however, it was included in this analysis to provide realistic estimates for a man-rated vehicle TPS aerocapturing at Mars.

The 12.2 m AFE utilizes a high velocity (12 km/s) Earth aerocapture trajectory similar to that used by the SRC. For the Earth aerocapture, the uncertainties in guidance, navigation, and atmospheric characteristics are more acceptable, and the AFE design can be used with confidence for this trajectory.

The altitude, velocity, and pressure as a function of time for the SRC are shown in figures 2, 3, and 4, respectively, along with the LTVs and AFE. From these figures it can be seen that the Mars return vehicles enter at higher velocity and penetrate shallower into the atmosphere than the same corresponding class LTV: 68.9 km for the SRC, and 72 km for the AFE. At Mars the AFE's minimum altitude was 42.8 km, a difference of almost 30 km, even though the maximum stagnation pressure was approximately the same (5.25×10^{-2} atm at Mars versus 3.46×10^{-2} atm at Earth).

Aerodynamic Heating

After the trajectory has been defined for the vehicles being analyzed, the aerothermodynamic (convective/radiative) heating environment can be predicted. Usually, to a first-order approximation, the programs used to determine trajectories can provide stagnation heating rate values; however, the analysis used in this investigation required an approximation to the two-dimensional (2-D) and 3-D effects for real gas (air or CO₂). A heating distribution for an equilibrium flow approximating a fully catalytic surface at the peak heating condition was used. Selected time points were used to define the convective and radiative stagnation heating for the entry trajectory.

The MINIVER¹⁹ program was used to calculate the initial approximation of the convective heating rates for the LTV trajectories. The MINIVER program is able to approximate heating to simple geometric shapes once the free stream properties have been defined either by input or trajectory and atmosphere. It was used to define the stagnation heating to the reference spheres for a fully catalytic surface using the method of Fay and Riddell.²⁰ For the raked cone an effective radius of 7.2 m was used; 0.9 m and 2.2 m were used for the SRC and scaled-up Apollo CM; 5.3 m and 4.3 m were used for the domed cylinders; and 6.6 m for the AFE.

The Boundary Layer Integral Matrix Procedure (BLIMP) computer program²¹ was used to determine the convective stagnation heating rate for these vehicles and the QRAD program was used to calculate the radiative heating for Earth entry. BLIMP computes the heating based on the nonsimilar chemically reacting laminar or turbulent boundary layer. The BLIMP calculations may be performed for either local thermodynamic equilibrium, fully catalytic wall or for nonequilibrium flow with a partially catalytic wall. The MINIVER data used by BLIMP were the stagnation enthalpy and pressure. The stagnation enthalpy, h_{stag}, is calculated as

$$h_{stag} = \frac{V_\infty^2}{2gJ} + h_\infty + \sum_i a_{i\infty} \Delta h_i^0$$

where the subscripts stag and ∞ refer to stagnation and free stream conditions. The subscript i refers to the individual species, the heat of formation is represented by Δh_i^0 , and the $a_{i\infty}$ are the mass fractions for the individual species.

An equilibrium flow condition was used to calculate the convective heating to establish mass fractions at the boundary layer edge. For Earth entry, mass fractions were calculated for five species: O, O₂, N, N₂, and NO. In air, the heat of formation is zero for N₂ and O₂, and the stagnation enthalpy is a function of only velocity and altitude.

A wall temperature iteration program was developed for BLIMP such that the radiation equilibrium temperature, T_{re}, was computed at each station based on the sum of the convective heating rate, q_c, and radiative heating rate, q_r, as

$$T_{re} = \left(\frac{\dot{q}_c + \dot{q}_r}{\sigma \epsilon} \right)^{1/4}$$

The MINIVER data used by the QRAD program were the altitude, relative velocity, free stream density, stagnation enthalpy, and stagnation pressure. The QRAD program uses the sum of the equilibrium and nonequilibrium air radiation. The equilibrium method uses a four band model (infrared (IR) lines, visible continuum, ultraviolet (UV) lines, and UV continuum). The nonequilibrium model includes binary scaling (velocity dependent), and is collision limited at

high altitudes. Both models include radiation cooling, self absorption of UV, and 3-D effects. The BLIMP program was used to calculate the heating distribution at peak heating conditions. Additional discussion on the aerodynamic heating analysis for these vehicles can be found in a paper by Rochelle, et. al.²²

A gradual solar heating buildup to 4.54×10^{-2} w/cm² at 5000 seconds was assumed for all surfaces as the vehicle exited the Earth's atmosphere after the aeropass. This solar heating then decayed linearly to 2.27×10^{-2} w/cm² at 10,000 seconds to represent a managed solar thermal environment. Typically, bond line and structure temperatures exhibit little change from the initial conditions at the time of maximum surface heating and reach their peaks during the long soak back when the surface heating and structural loads are minimal.

The convective, radiative, and total heating (convective and radiative) at the stagnation point for the vehicles entering the Earth's atmosphere can be seen in figures 8, 9, and 10, respectively. For the raked cone it can be seen that the convective heating is approximately 50% greater than the radiative heating for a peak combined heating of 71.2 w/cm². It can also be seen that the radiative heating drops off more rapidly after peaking than the convective heating. For the modified CM it can be seen that the convective heating is approximately the same magnitude as the radiative heating for a peak combined heating of 244.1 w/cm². The radiation peaks approximately 4 seconds earlier than the convective heating. It can also be seen that the radiative heating drops off more rapidly after peaking than the convective heating.

Similarly, for the domed cylinder vehicles it can be seen that the convective and radiative heating are approximately the same magnitude, although the peaks are at slightly different times. As with the modified CM and raked cone, the radiation heating decays more rapidly than the convective heating. The greatest convective heating was developed for the SRC (223.9 w/cm²). Due to its smaller effective radius, the radiation heating (36.9 w/cm²) was approximately the same as for the lowest of the domed cylinders (38.0 w/cm²).

A summary of the peak heating conditions for these vehicles can be found in table II. A summary tabulation of the stagnation point heating and pressure data for these vehicles can be found in table III.

The BLIMP computer program was also used to determine the convective stagnation heating rate for the biconic trajectories for Mars entry. The heating rates were calculated for equilibrium flow with BLIMP assuming a 100% CO₂ atmosphere. Mass fractions were calculated for five species: C, O, CO, CO₂, and O₂. As opposed to air, the heat of formation for CO₂ is -94,052 cal/mole, and the third term is significant in the stagnation enthalpy calculation.

The Radiating Inviscid Flow Stagnation Point Program²³ (RIFSP) developed by Sutton, was used to calculate radiation heating rates for the biconic vehicles. The method employed by RIFSP is based on a radiatively coupled solution of the inviscid flow equations at the stagnation of a hemisphere.⁶ The radiation model is coupled to the RAD/EQUIL program developed by Nicolet.²⁴ This radiation model includes the atomic line, continuum, and molecular band transitions from UV to IR. This nongray radiative method calculates the absorption coefficient as a function of the wavelength. Additional discussion of the aerodynamic heating analysis for these vehicles can be found in the paper by Rochelle, et al.²²

The convective, radiative, and total heating rates for the Mars biconic vehicles are shown in figures 11, 12, and 13, respectively. The peak stagnation heating was 44.2 w/cm², 121 w/cm², 237 w/cm², and 456 w/cm² for the 6 km/s, 8 km/s, 10 km/s, and 12 km/s trajectories, respec-

tively, assuming a 0.61 m R_N . For the 0.3 m R_N 6 km/s trajectory, the peak heating was 62.5 w/cm². The radiative heating for the vehicle entering at 6 km/s was negligible, but for higher velocities the contribution from radiation cannot be ignored. The peak radiative heating rate for the vehicle entering at 8 km/s was 8.9 w/cm², at 10 km/s it was 34.2 w/cm² (14.4% of the convective heating), while for the biconic entering at 12 km/s, the radiative heating increased to 338.7 w/m² (73% of the convective heating). The 12.2 m AFE had a peak convective, radiative, and combined heating of 31.7 w/cm², 19.5 w/cm², and 51.2 w/cm², respectively.

For both the Mars entry and Earth entry analyses, it was assumed that the radiative and convective heating calculations were uncoupled. Also, the effects of ablation products on reducing the radiative heating were not considered.

A gradual solar heating buildup to 4.54×10^{-2} w/cm² at 5000 seconds was assumed for all surfaces as the vehicle exited the Martian atmosphere after the aeropass. This solar heating then decayed linearly to 2.27×10^{-2} w/cm² at 10,000 seconds to represent a managed solar thermal environment. A summary tabulation of the peak heating conditions for these vehicles can be found in table II. A summary tabulation of the stagnation point heating and pressure data for these vehicles can be found in table IV.

The BLIMP program was used to calculate the convective heating distribution at peak heating conditions using the methods described earlier for the vehicles entering the Earth's atmosphere. For all vehicles except the Apollo-shaped vehicles, the radiative heating distribution was assumed to be the same as the convective heating distribution. In addition to the data requirements mentioned previously, pressure distributions were obtained at peak heating conditions for each vehicle. The raked cones pressure distribution is based on an inviscid nonequilibrium Euler solution calculated by Gomez.²⁵ The domed cylinder's pressure distribution was calculated by Stuart.²⁶ Pressure distributions for these vehicles can be seen in figure 14. The pressure distributions for the Apollo-shaped vehicles were not used since the heating distribution data were assumed to be the same as for the original CM.

The convective heating distribution data were taken from figures presented by Lee, Bertin, and Goodrich¹⁷ and the radiative heating distribution data were taken from Ried, Rochelle, and Milhoan.³ The heating distribution for the AFE was assumed to be the same as for the original AFE.²⁷ Heating distribution curves for these vehicles are presented in figure 15. The data for the Apollo-shaped vehicles in figures 14 and 15 are actually a function of S/R instead of the S/L shown for the abscissa.

The BLIMP program was used to calculate the heating distribution at peak heating conditions using the methods described earlier for the vehicles entering the Mars atmosphere. Pressure distributions were calculated by Stuart at peak heating conditions for the 0.3 m R_N biconic vehicle entering at 6 km/s and for the 0.61 m R_N biconic vehicle entering at 8 km/s for a CO₂ atmosphere.²⁸ These pressure distributions can be seen in figure 16. The heating distributions calculated for the 8 km/s trajectory were assumed to be valid for trajectories for all 0.61 m R_N biconics, see figure 17. The same heating distribution used at Earth was used at Mars for the AFE.

Turbulent flow heating was not included in this analysis as the values of Re_θ were less than 300 for all vehicles considered. For the Shuttle Orbiter, transition was not observed to occur until a value of approximately 400 was obtained for Re_θ .²⁹

TPS Materials

Thermal protection systems were designed for these vehicle configurations using state-of-the-art materials with an energy weight fraction calculated to show whether aerocapture was a viable alternative to an all-propulsive capture. The TPS design analysis is concerned only with the short period of dominant heating during the atmospheric aeropass and subsequent thermal soakback.

As was mentioned earlier, the ground rules for this analysis permitted use of material technology that should be available within the next decade. The ground rules also called for a composite material for the aeroshell structure.

The assumptions made in the material selection for this analysis are based on anticipated surface temperatures. For all vehicles where a Reusable Surface Insulation (RSI) material cannot be used due to material temperature limitation, an ablator, AVCO-5026-H/CG, was used. AVCO-5026-H/CG is a charring ablator that was used for thermal protection on the Apollo CM. Due to its use during the Apollo program, more detailed knowledge exists for this material than any other ablator. It consists of phenolic microballoons embedded in a Novolac resin which is formed in phenolic honeycomb cells. It has a virgin density of 513 kg/m^3 and a char density of 320 kg/m^3 .

For the reusable LTVs, however, it is assumed that a material similar in thermophysical properties to Advanced Carbon/Carbon (ACC) will be available to withstand the surface temperatures above 1927°C . For this analysis it was assumed that the carbon/carbon system was seven plies thick (0.229 mm). The secondary thermal insulation selected for this system was a Cerachrome blanket with a nominal density of 192 kg/m^3 . It is assumed that the Cerachrome will be tied to the structure and that good thermal contact will be maintained throughout the flight regime. It should be stressed that it is not proposed that the current state of development would permit ACC to be used at these elevated temperatures (above 1649°C), but it is anticipated that by the end of the decade a material with similar thermophysical properties to ACC could be developed and used for spacecraft design at these temperatures. This New Advanced Carbon/Carbon material will be referred to as NACC.

For surface temperatures between 1483°C and 1927°C , it was assumed that a material similar to FRCI-12 could be used. FRCI-12 is coated with reaction cured glass (RCG) and has a surface emissivity of 0.85. This coating is 0.0381 cm thick, and the minimum thickness for FRCI-12 with the coating is 0.813 cm. FRCI-12 has a nominal density of 192 kg/m^3 . This new Rigid Fibrous Ceramic material will be referred to as RFC. It should be stressed that we are not proposing that the silica-based material, FRCI-12, will be used at temperatures above 1483°C , but rather we are suggesting, as with NACC, that an alternate RFC material, possibly zirconium, could be developed that would have thermophysical properties similar to those possessed by FRCI-12, and be capable of operating at these elevated temperatures.

Unlike Cerachrome, the ceramic materials are bonded to a NOMEX felt, which is bonded to the structure. The felt acts as a Strain Isolation Pad (SIP) between the insulator and structure. RTV-560 is assumed to be the bonding adhesive. RTV-560 has a temperature service limit of 288°C while NOMEX felt has a temperature service limit of 444°C (thermophysical property values are tabulated up to 538°C). Thus, the temperature service limit for the SIP is constrained to 288°C . The assumed thickness for the RTV-560 and felt are 0.1905 mm and 4.064 mm, respectively. The TPS materials used in this analysis and their assumed service temperature limits are shown in table V.

Another advanced ceramic material used for TPS design is a high temperature performance material (96.1 kg/m^3) designated as HTP-6. HTP-6 was used in those areas where a minimum LI-900 material thickness was predicted. All materials except HTP-6, NACC, and RFC are flight certified. Standard data book conductivity values were used for aerocapture at Earth, and calculated conductivity values for RFC, FRCI-12, LI-900, and HTP-6 in a CO_2 atmosphere were used for the Mars aerocapture. FRCI-12 and RFC conductivity values were extrapolated from 927°C to 1649°C in air and CO_2 . The thermal response of these materials is a function of density, temperature, and pressure. The thermal response of NOMEX felt is also sensitive to changes in temperature and pressure but no attempt was made to calculate the conductivity in a CO_2 atmosphere for this material.

Sensitivity to pressure is particularly important for aeropass TPS design since most of the heating occurs at pressures below 7.9×10^{-2} atmospheres for the reusable LTVs; below 5.9×10^{-2} atmospheres for the AFE; the 6 km/s and 8 km/s biconics; and below 1.8×10^{-2} atmospheres for the 10 km/s and 12 km/s biconics (see figures 4 and 7).

Structural Materials

The material selected for use in the thermal analysis for the LTVs and AFE consisted of a lightweight honeycomb composite consisting of graphite epoxy face sheets with a NOMEX paper honeycomb core (G/E Honeycomb). The structure design parameters are two 0.4064 mm graphite epoxy face sheets sandwiching the 3.81 cm honeycomb core with a maximum use temperature of 177°C .

The aeroshell for each LTV was sized for Earth entry³⁰ with the thrust structure accounted for in the dry mass vehicle sizing program. Time did not permit the integration of the aeroshell and thrust structures to optimize structure mass. Most designs had a 1.4 factor of safety using the graphite epoxy honeycomb structure. The structure for the CM was scaled up from the original Apollo CM from data provided by Heineman.³¹

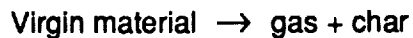
The structural materials used for the biconics and SRC were Graphite Epoxy (G/E) and aluminum. The G/E structure was used behind the ablator portion of the biconic vehicles, and has a maximum reuse temperature of 316°C . The structure used for the RSI materials on the biconic vehicles consisted of a 1.016 mm thick aluminum plate. This was found to provide the lowest TPS weight penalty of all of the structures considered in the previous MRSR paper. The maximum reuse temperature limit for the aluminum was 288°C . For the 12.2 m modified AFE, the same aeroshell structure used by the LTVs was assumed.

TPS Sizing

The AESOP-STAB thermal analysis program³² was used to calculate the minimum weight TPS for the ablative system and the AESOP-THERM thermal analysis program³³ was used to calculate the minimum weight TPS for RSI materials. Typically, the minimum weight condition is subject to temperature constraints imposed on the backwall of selected materials. These programs are actually segregated into two parts: the optimization portion which controls the numerical process to minimize the TPS subject to the temperature constraints, and the thermal analysis portion which calculates the thermal response of the system subject to the initial and boundary conditions. Since only one material was permitted to vary in this analysis a simple quadratic fit was selected for material minimization.

The response of a charring ablation material to a high velocity, hyperthermal atmospheric entry environment is the result of complex physicochemical processes. A sketch of a simplified physical system for the charring ablator can be seen in figure 18.

The basic ablation mechanism modeled in the AESOP-STAB program is the pyrolysis of ablative material described by the expression



This process is assumed to occur in the "reaction zone" defined by temperature and density limits.

In addition to the basic pyrolysis of virgin ablator, the following energy transport mechanisms may occur

- transport by convection of the pyrolysis gases through the porous char,
- transport by conduction throughout the entire system,
- transport by reactions between the char and pyrolysis gas products such as redeposition of pyrolysis gas products on the char structure (coking) and reactions between char and pyrolysis gas constituents.

A sketch of the surface energy balance can be seen in figure 19.

Mathematically, the program is structured so the ablator must be attached to a backup material or carrier plate. Subsequent material backwall boundary conditions include: adiabatic, perfect thermal contact with another material, air gap with or without fluid flow, and a cabin sink.

The nonablating thermal model (AESOP-THERM) also incorporates these boundary conditions. Both programs incorporate a technique that bounds the surface temperature.³⁴ Sketches of representative thermal models used for reusable materials can be seen in figure 20, and for the ablator in figure 21.

TPS sizing techniques, as described by Williams, et al.,³⁵ were employed in this analysis to assess the relative performance of the various insulation systems. The nondimensional heating distributions used in this analysis are shown in figures 15 and 17. As an additional aid in material selection it is convenient to view the predicted radiation temperature (T_{re}) as a function of the wetted length at the peak heating conditions. This can be calculated by using the peak heating and heating distribution curves. A representative curve used in the LTV analysis can be seen in figure 22.

For the biconic vehicles aerocapturing at Mars the 0.61 m R_N vehicle design with current materials, and the 0.3 m R_N vehicle with advanced TPS materials entering at 6 km/s will not require the use of an ablator. In contrast, for the 12 km/s trajectory the entire lower surface will require an ablator to protect the structure. Likewise, for the modified AFE an ablator will be required at both Mars and Earth. This dual entry presents an additional complication in that the analysis for Earth aerocapture requires that the ablator enter with an initial char and surface recession established at Mars. All other ablation analyses initiate entry assuming a virgin ablator.

The 0.61 m R_N vehicle entering Mars at 6 km/s did not require an ablator. If the advanced ceramic, RFC, with a 1927°C temperature limit is available, then an ablator will not be required

for the 0.3 m R_N vehicle entering at 6 km/s. All other biconic vehicles will require an ablator in the region of high heating. Minimum TPS unit weights were calculated, subject to temperature constraints, for several heat factors for RFC, FRCI-12, and LI-900. The minimum material condition (MMC) assumed for this analysis was 0.81 cm for the RSI and ablator on SIP, and either 1.26 cm or 0.81 cm for the ablator without SIP, depending on whether RSI material exists downstream of the ablator. FRSI is considered for use in areas where the surface temperature is calculated to be under 371°C.

In a similar manner, it can be seen that the modified AFE will require an ablator both at Mars and Earth. A comparison of the peak heating rates and radiation equilibrium temperatures for all vehicles analyzed can be seen in table II.

Since the 12.2 m AFE performs two aerocaptures, the analysis is unlike previous analyses, i.e., considering only one aerocapture. Identical heat factor distributions were assumed at both Mars and Earth, and the sizing for the RSI materials is straightforward. The optimum TPS unit weights were calculated for each material at several heat factors for both Mars and Earth aerocaptures. Then, for each heat factor, the maximum between Mars and Earth optimum thicknesses were selected for the design thickness.

The ablation analysis for this vehicle, however, required a two-step process. AESOP-STAB analysis runs were performed at Mars and Earth. Some surface recession and mass loss were predicted at Mars. The recession and char depths were established as initial conditions for the Earth aerocapture. Thermophysical properties for the charred ablator were identical at both Mars and Earth. The density in the region in the ablator between total char and virgin material was approximated by the method described in the AESOP-STAB update.³⁶ With these initial conditions the optimum ablator thickness was calculated for each appropriate heat factor. Ablator thicknesses were also calculated at Mars to ensure that a thicker ablator would not be required for the Mars aerocapture.

Only thermal response of the ablator at Earth will be discussed since it is where the critical sizing is required, although some comparison will be made with the heating and ablation at Mars. The response of the ablator at the point of maximum heating (stagnation point) during the Mars aerocapture can be seen in figure 23, which shows the temperature time history of the ablator surface, ablator backwall, and G/E Honeycomb backwall for the first 2000 seconds. From this figure it can be seen that the peak surface temperature was approximately 1266°C. The ablation rate for this heating can be seen in figure 24.

In figure 25 the corresponding thermal response can be seen for the aerocapture after the return to Earth from Mars. The peak surface temperature of 1805°C occurred around 70 seconds while the peak on the G/E face sheet occurred much later in time, around 4500 seconds. The 316°C isotherm reached a depth of 1.84 cm, the 538°C isotherm maximum depth was 1.37 cm, and the 1024°C isotherm maximum depth was 0.84 cm.

The initial char values are not zero since some mass loss was calculated to occur at Mars (see figure 26). The initial values differ slightly from the values calculated from the Mars aerocapture which were 0.79 cm (0.9 char ratio) and 0.56 cm (0.1 char ratio). The approximation to the density between char ratios of 0.0 and 1.0 produced an error of 7% at the 0.9 char density ratio, and is within an acceptable tolerance level since the density curve is relatively flat in this region.

For the Earth aerocapture, the 0.1 and 0.9 char density ratio depths were 1.23 cm and 1.49 cm, respectively. This approximation started with an initial recession of 0.18 mm due to the Mars

aerocapture, and achieved a maximum recession depth of 0.58 mm at approximately 200 seconds. It is interesting to observe that maximum ablation rate at Earth was slightly less than that calculated at Mars even though the surface temperature was approximately 540°C greater than that at Mars (see figures 24 and 27). This probably can be attributed to the pre-char condition that exists at Earth for the returning vehicle.

Weight Analysis

The TPS penalty factors used in this analysis η_T , η_S , and η_{TS} are defined as:

$$\eta_T = \frac{100 \text{ TPS weight}}{\text{Total vehicle weight}}$$

$$\eta_S = \frac{100 \text{ Structural weight}}{\text{Total vehicle weight}}$$

$$\eta_{TS} = \eta_T + \eta_S.$$

where the structural weight consists of the aeroshell and any rings, stringers, or stiffeners required.

Determination of a vehicle weight is a very complicated iterative process, especially during the early stages of the preliminary design. Initially, the weight is used as one of the characteristic parameters for designing the trajectory and vehicle geometry. No growth contingency factors are provided for TPS weights or temperatures in this paper.

The thermal analysis results are summarized in figures 28 and 29 which show the typical heat load versus TPS unit weight curves for the biconics and LTVs. In these plots the corresponding weight for each TPS analyzed is shown for direct comparison. It is interesting to observe not only the large difference between the classes of thermal protection systems (ablator, carbon/carbon, and the low weight insulators), but the comparison between the low weight insulators. From these figures it can be seen that the TPS unit weight for HTP-6 is less than that of LI-900 only at the minimum material conditions (MMC) of 0.813 cm for the tiles. LI-900 was consistently lighter than all other insulators until MMC was achieved.

Gomez,²⁵ Stuart,²⁶ and Robinson³⁷ provided cumulative area distributions as a function of S/L for the raked cone, domed cylinders, and 12.2 m AFE. From the TPS unit weights, along with the area distributions, the TPS weights can be calculated for each vehicle, and hence, the weight penalty. The results of these calculations are summarized in figure 30, which shows the TPS weight penalty for all Earth entry vehicles analyzed as a function of angle-of-attack, and figure 31 which shows the weight penalty for the biconics and 12.2 m AFE as a function of entry velocity at Mars. Figure 32 shows the TPS weight penalty as a function of the ballistic coefficient ($m/C_L S$) for all vehicles; however, this tends to obscure the data for the biconics.

It should be observed that for the raked cone and the domed cylinder entering at $\alpha = 57^\circ$, only the advanced RFC material was required. The NACC system was not required. Likewise, for the MRSR vehicles the 0.3 m R_N vehicle could have been developed using a carbon/carbon system (no margin) without resorting to advanced material technology, and to an all RSI system using advanced material technology. In contrast, the 0.61 m R_N biconic entering at 6 km/s can be designed with a low weight RSI TPS using current material technology.

Figure 33 shows the relationship between η_S and η_T for each vehicle to arrive at the total weight penalty η_{TS} . It is interesting to observe that the driving penalty factor for the LTVs is due to the

inherent structure required to support the TPS. In a similar vein, figure 34 shows the same information with a 20% uncertainty factor included. Even with the uncertainty factor a majority of the vehicles had a total TPS weight penalty, η_{TS} , of less than 25%. Typical results for the high angle-of-attack domed cylinder and 12.2 m AFE can be seen in figures 30 through 32. The weight penalty of 16% for the raked cone yields a 77% increase in payload over an all-propulsive stage for a lunar surface to LEO mission. This approximation to increase in payload is taken from Roberts¹ and is duplicated in figure 35. For the domed cylinder entering at 57° the savings are even greater; the 15% weight penalty yields a 78% increase in payload.

The weight penalty for the MRSR vehicles appears to increase by approximately 7% for each 2 km/s increase in relative velocity, but if advanced material technology can be used this increase can be cut in half, see figure 31. The most economical ablative system appears to be one with SIP under the ablator. Even at 12 km/s the total TPS weight penalty was only 22%. This is approximately the same magnitude as for the expendable 4.37 m CM analyzed for the LTV missions.

The 12.2 m AFE had an η_{TS} of 20.2% using current material technology and 11.4% using advanced material technology, which is less than half of that required for the unmanned SRC previously analyzed.

An overall comparison of the advantages that can be gained using aerobraking can be summarized by only considering the percent increase in payload over an all-propulsive system. In table VI these benefits are summarized for the three vehicle classes (AFE, biconic or domed cylinder, and Apollo CM) that were studied in this analysis. Graphically, this same information is presented in figure 36. It is fairly interesting to observe that reusable vehicles tend to provide a greater increase in payload than expendable vehicles, and all vehicles can provide an increase in payload of 50% to 85% over an all-propulsive system

Also of interest is the relationship between the surface area and weight for each TPS. This is illustrated graphically in figures 37 and 38 for the 57° Domed Cylinder. In this case, the RFC covers 42% of the TPS surface and consists of 74.8% of the TPS weight. In direct contrast FRSI covers 44.2% of the surface area, but contributes only 10.7% to the total TPS weight. Similarly, in figures 39 and 40, the relative TPS areas and mass for the 10 km/s Biconic can be seen. These two figures show the relative proportion for the different insulation materials using current material technology for an ablative TPS. In this case, the ablator covers 14.2% of the surface area and contributes to 34.1% of the TPS weight. LI-900 covered 84.5% of the surface, but contributed to only 63.7% to the TPS weight.

Concluding Remarks

An investigation was made for 5 crew-carrying LTVs, 5 unmanned MRSRs, and one crew-carrying vehicle that aerobraked at Mars and returned to aerobrake at Earth. For each vehicle analyzed, aerobraking was determined to be more efficient than an all-propulsive system.

A comparison was made against different competitive TPS designs for LTVs. Three of the reusable LTV designs were more efficient than for the expendable design: the raked cone and the two high angle-of-attack domed cylinders. Of these, the two domed cylinders were slightly more efficient than the raked cone, with the 57° angle-of-attack vehicle yielding the lowest η_{TS} (15.1%).

Five unmanned MRSR vehicles were analyzed and the most efficient, with respect to η_{TS} , was the 0.61 m R_N biconic aerobraking at the lowest, 6 km/s, relative velocity. If the relative velocity

is doubled the vehicle can still be designed with a weight penalty of less than 27% using current material technology, and less than 23% using advanced material technology. While these systems will require an ablator, it does demonstrate that the transit time can be reduced while maintaining the inherent advantages of an aerobraking TPS.

A vehicle sized to carry a crew and supplies, the 12.2 m AFE, was analyzed for an aerocapture at Mars followed by an aerocapture at Earth. The results of this analysis indicated that the TPS is sized primarily by the Earth aerocapture, and demonstrates that aerobraking is a viable alternative to an all-propulsive system for a large vehicle. Assuming advanced material technology, a weight penalty, η_{TS} , of 11% was achieved, whereas if current material technology is used the weight penalty is 20%. If alternate vehicle designs were analyzed the weight penalty could possibly be reduced even further.

References

1. Roberts, B. B.: Systems Analysis and Technology Development for the NASA Orbit Transfer Vehicle. AIAA-85-0965, AIAA 20th Thermophysics Conference, Williamsburg, VA; June 19-21, 1985.
2. Lee, D. B.; and Goodrich, W. D.: The Aerothermodynamic Environment of the Apollo Command Module During Superorbital Entry. MSC-05873, NASA Manned Spacecraft Center, Houston, TX; January 1972.
3. Ried, R. C., Jr.; Rochelle, W. C.; and Milhoan, J. D.: Radiative Heating to the Apollo Command Module: Engineering Prediction and Flight Measurement. NASA TM X-58091, NASA Manned Spacecraft Center, Houston, TX; April 1972.
4. Marvin, J. G. and DeWert, G. S.: Convective Heat Transfer in Planetary Gases. NASA TR R-224, NASA Ames Research Center, Moffet Field, CA; 1965.
5. Sutton, K. and Graves, R. A., Jr.: A General Stagnation Point Convective Heating Equation for Arbitrary Gas Mixtures. NASA TR- R-376, NASA Langley Research Center, Hampton, VA; November 1971.
6. Sutton, K.: Characteristics of Coupled Nongray Radiating Gas Flows With Ablation Products Effects About Blunt Bodies During Planetary Entries. NASA TMX-72078, NASA Langley Research Center, Hampton, VA; 1973.
7. Tauber, M. E.; Palmer, G. E.; and Yang, L.: Earth Atmosphere Entry Studies for Manned Mars Missions. AIAA-90-1699, presented at AIAA/ASME 5th Joint Thermophysics and Heat Transfer Conference, Seattle, WA; June 18-20, 1990.
8. Tauber, M. E.; Bowles, J. V.; and Yang, L.: The Use of Atmosphere Braking During Mars Missions. AIAA-89-1730, presented at AIAA 24th Thermophysics Conference, Buffalo, NY; June 12-15, 1989.
9. Park, C.; Howe, J. T.; Jaffe, R. L.; and Candler, G. V.: Chemical-Kinetic Problems of Future NASA Missions. AIAA-91-0464, presented at 29th Aerospace Sciences Meeting, Reno, NV; January 7-10, 1991.

10. Gupta, R. N.; Sutton, K.; Moss, J. N.; and Lee, K. P.: Viscous-Shock-Layer Solutions With Coupled Radiation and Ablation Injection for Earth Entry. AIAA-90-1697, presented at AIAA/ASME 5th Joint Thermophysics and Heat Transfer Conference, Seattle, WA; June 18-20, 1990.
11. Carlson, L. A.; and Gally, T. A.: The Effect of Electron Temperature and Impact Ionization on Martian Return AOTV Flowfields. AIAA-89-178, presented at AIAA 24th Thermophysics Conference, Buffalo, NY; June 12-14, 1989.
12. Williams, S. D.; Pavlosky, J. E.; and Curry, D. M.: A Preliminary TPS Design for MRSR - Aerobraking at Mars and at Earth. AIAA-90-0052, presented at 28th Aerospace Sciences Meeting, Reno, NV; January 8-11, 1990.
13. Henline, W. D.: Aerothermodynamic Heating Environment and Thermal Protection Materials Comparison for Manned Mars-Earth Return Vehicles. AIAA-91-0697, presented at AIAA 29th Aerospace Sciences Meeting, Reno, NV; January 7-10, 1991.
14. Williams, S. D.; Rochelle, W. C.; Bouslog, S. A.; Ting, P. C.; Colovin, J. E.; and Gietzel, M. M.: A Preliminary TPS Design for Two Aerobraking Lunar Return Vehicles. LESC-28103, Lockheed Engineering and Sciences Co., Houston, TX; February, 1990.
15. Williams, S. D.; Bouslog, S. A.; Gietzel, M. M.; Rochelle, W. C.; and Colovin, J. E.: A Preliminary TPS Design For Expendable/Reusable Aerobraking Lunar Return Vehicles. LESC-28329, Lockheed Engineering and Sciences Co., Houston, TX; May, 1990.
16. Williams, S. D.; and Gietzel: An Update to the Preliminary TPS Design for Vehicles Aerobraking at Mars and at Earth. LESC-28888, Lockheed Engineering and Sciences Co., Houston, TX; October, 1990.
17. Lee, D. B.; Bertin, J. J.; and Goodrich, W. D.: Heat-Transfer Rate and Pressure Measurements Obtained During Apollo Orbital Entries. NASA TND-6028; October 1970.
18. Scott, C. D.; Roberts, B. B; Nagy, K.; Taylor, P.; Gamble, J.; Cerimeli, C. J.; Kroll, K. R.; Li, C. P.; and Ried, R. C.: Design Study of Aerobraking Orbital Transfer Vehicles. NASA TM-58264, NASA JSC, Houston TX; March 1985.
19. Hender, D. R.: A Miniature Version of the JA70 Aerodynamic Heating Computer Program, H800 (MINIVER). MDC G0462, McDonnell Douglas Astronautics Company; Huntington Beach, CA; June 1970, revised January 1972.
20. Fay, J. A.; and Riddell, F. R.: Theory of Stagnation Point Heat Transfer in Dissociated Air. J. Aerospace Science, Vol. 25, No. 2, pp. 73-85; 1958.
21. Murray, A. L., Further Enhancements of the BLIMP Computer Code and User's Guide. AFWAL-TR-88-3010, Wright-Patterson Air Force Base, OH; June 30, 1988.
22. Rochelle, W. C.; Bouslog, S. A.; Ting, P. C.; and Curry, D. M.: Aerothermodynamic Environments for Mars Entry, Mars Return, and Lunar Return Aerobraking Missions. AIAA 90-1701, presented at the AIAA/ASME 5th Joint Thermophysics and Heat Transfer Conference, Seattle, WA; June 18-20, 1990.

23. Sutton, K.: Air Radiation Revisited. AIAA -84-1733, presented at the AIAA 19th Thermophysics Conference, Snomass, CO; June 25-28, 1985.
24. Nicolet, W. E.: Advanced Methods for Calculating Radiation Transport in Ablation Product Contaminated Boundary Layers. NASA CR-1656, September 1970.
25. Gomez, R. J.: Undocumented Communication on the Lunar Return Aerocapture Analysis Results for the Raked Cone. JSC Advanced Programs Office, January, 1990.
26. Stuart, P. C.: Undocumented Communication on the Lunar Return Aerocapture Analysis Results for the Domed Cylinder. JSC Advanced Programs Office, January - May 1990.
27. Rochelle, W. C.; Ting, P. C.; Mueller, S. R.; and Colovin, J. E.: Data Book Documentation - AFE Aerobrake Aerothermodynamic Data Book For Baseline V Trajectory, Volume I - Pitch Plane. JSC-23623, LESC-26950, Lockheed Engineering & Sciences Co., Houston, TX; April 1989.
28. Stuart, P. C.: Undocumented Communication on the MRSR Aerocapture Analysis Results for the Biconic Vehicles. JSC Advanced Programs Office, October 1989.
29. Goodrich, W. D.; Derry, S. M.; and Bertin, J. J.: Shuttle Orbiter Boundary Layer Transition at Flight and Wind Tunnel Conditions. Presented at Langley Conference on Shuttle Performance: Lessons Learned, Hampton, VA, March 1983, pp. 753-779.
30. Verinder, I. E.: LTV Structural Design Presentation. NASA/JSC, Houston, TX; January 31, 1990.
31. Heineman, W. Jr.: Undocumented Communication on Apollo Dimensions and Shape. JSC Systems Engineering Division, April 1990.
32. Williams, S. D.: Revised Users' Guide to the AESOP-STAB Computer Program - Cray Version. LESC-29161, Lockheed Engineering and Sciences Company, Houston, TX; January 1991.
33. Williams, S. D.: Users' Guide to the AESOP-THERM Computer Program - Cray Version. LESC-28949, Lockheed Engineering and Sciences Company, Houston, TX, November 1990.
34. Williams, S. D.; and Curry, D. M.: An Implicit - Iterative Solution of the Heat Conduction Equation with a Radiation Boundary Condition. International Journal for Numerical Methods in Engineering, Vol. 11, No. 10, 1977, pp. 1605-1619.
35. Williams, S. D.; Rochelle, W. C.; Bouslog, S. A.; Ting, P. C.; Colovin, J. E.; and Gietzel, M. M.: A Preliminary TPS Design for Two Aerobraking Lunar Return Vehicles. LESC-28103, Lockheed Engineering and Sciences Co., Houston, TX; February, 1990.
36. Williams, S. D., and Gietzel, M. M., AESOP-STAB Update - Initializing the Thermal Model with Initial Char and Mass Loss. LESC-27439, Lockheed Engineering and Science Co., Houston, TX; August 28, 1989.

37. Robinson, T. S.: Undocumented Communication on the Cumulative Area Distributions for AFE Vehicles as a Function of S/L. Lockheed Engineering and Sciences Co., Houston, TX; August, 1990.

Table I - Basic Vehicle and Trajectory Design Parameters

Vehicle	Description	Entry mass kg	Relative Velocity km/s	L/D	α deg	γ deg	$m/C_L S$ kg/m ²
SRC	1.8m Diam. Mars Return	329	11.8	0.280	20	-5.7	1358.3
Scaled-Up Apollo CM	4.4m Diam. LTV	7,938	10.6	0.300	20	-5.7	1358.3
Raked Cone	18.3m x 14.6m Modified AFE- LTV	26,630	10.6	0.350	17*	-5.1	311.5
Domed Cylinder	10.7m Diam. 22.86m Long - LTV	28,217	10.6	0.500	40	-5.2	409.1
Domed Cylinder	8.5m Diam. 19.81m Long - LTV	29,837	10.6	0.407	55	-5.7	548.3
Domed Cylinder	8.5m Diam. 19.81m Long - LTV	29,837	10.6	0.385	57	-5.5	555.6
Biconic	.3048m RN 9.906m Long - MRSR	5,001	5.9	1.000	27	-10.2	390.6
Biconic	.3048m RN 9.906m Long - MRSR	5,001	5.8	1.000	27	-10.2	390.6
Biconic	.6096m RN 9.906m Long - MRSR	5,001	5.8	1.000	20	-10.2	390.6
Biconic	.6096m RN 9.906m Long - MRSR	5,001	7.8	1.000	20	-11.4	390.6
Biconic	.6096m RN 9.906m Long - MRSR	5,001	9.8	1.000	20	-11.8	390.6
Biconic	.6096m RN 9.906m Long - MRSR	5,001	11.8	1.000	20	-12.1	390.6
AFE	12.2m Diam. Entry at Mars	22,680	7.8	0.280	17*	-11.0	511.2
AFE	12.2m Diam. Mars Return	13,151	11.7	0.280	17*	-5.1	296.4

* Angle of attack for Natural Trim, $\alpha = 0^\circ$ otherwise.

Table II - Peak Heating Conditions for the Vehicles

Vehicle	Description	α deg	Relative Velocity km/s	Convective Heating W/cm ²	Radiative Heating W/cm ²	Total Heating W/cm ²	T _{re} °C
SRC	1.8m Diam. Mars Return	20	11.8	223.8	36.9	260.7	2626
Scaled-Up Apollo CM	4.4m Diam. LTV	20	10.6	122.7	121.4	244.1	2395
Raked Cone	18.3m x 14.6m Modified AFE- LTV	17*	10.6	44.1	27.1	71.2	1688
Domed Cylinder	10.7m Diam. 22.86m Long - LTV	40	10.6	67.0	70.3	137.4	2038
Domed Cylinder	8.5m Diam. 19.81m Long - LTV	55	10.6	67.1	55.7	122.8	1974
Domed Cylinder	8.5m Diam. 19.81m Long - LTV	57	10.6	60.5	38.0	98.6	1853
Biconic	.3048m RN 9.906m Long - MRSR	27	5.9	99.9	0.0	99.9	1860
Biconic	.3048m RN 9.906m Long - MRSR	27	5.8	62.5	0.0	62.5	1625
Biconic	.6096m RN 9.906m Long - MRSR	20	5.8	44.2	0.0	44.2	1467
Biconic	.6096m RN 9.906m Long - MRSR	20	7.8	121.1	8.9	129.9	2004
Biconic	.6096m RN 9.906m Long - MRSR	20	9.8	237.0	34.2	271.1	2465
Biconic	.6096m RN 9.906m Long - MRSR	20	11.8	455.7	338.7	794.3	3310
AFE	12.2m Diam. Entry at Mars	17*	7.8	31.7	19.5	51.2	1532
AFE	12.2m Diam. Mars Return	17*	11.7	56.7	65.8	122.4	1972

* Angle of attack for Natural Trim, $\alpha = 0^\circ$ otherwise.

**Table III - Stagnation Point Heating and Pressure for
the Vehicles Aerocapturing at Earth**

1.8m SRC

Time seconds	Rad. Eq.			Temperature °C	Pressure Atmos.
	Convective w/cm ²	Radiative w/cm ²	Combined w/cm ²		
0.00	4.041	0.003	4.044	683.950	1.2785E-05
20.00	19.532	0.070	19.601	1146.500	2.9702E-04
30.00		0.676			1.4047E-03
40.00	83.108	1.282	84.391	1769.700	5.4404E-03
50.00	139.710	12.552	152.260	2080.500	1.5863E-02
55.00	167.170	29.201	196.370	2220.200	2.3482E-02
60.00	193.050	43.603	236.650	2330.800	3.2858E-02
65.00	213.700	54.849	268.550	2409.400	4.3047E-02
70.00	223.800	55.882	279.680	2437.900	5.1368E-02
75.00	221.990	49.107	271.090	2421.500	5.5809E-02
80.00	210.070	37.372	247.440	2368.000	5.5634E-02
90.00	177.380	15.185	192.570	2223.700	4.6376E-02
100.00	143.560	6.666	150.230	2080.500	3.6613E-02
105.00	131.530	4.199	135.730	2024.300	3.2998E-02
110.00	121.090	2.844	123.940	1974.200	3.0091E-02
120.00	104.970	1.457	106.420	1892.000	2.5782E-02
150.00	75.675	0.781	76.455	1720.800	1.8248E-02
200.00	42.638	0.238	42.876	1453.000	8.0300E-03
250.00	18.885	0.047	18.931	1134.400	1.7972E-03
300.00	8.016	0.009	8.024	862.710	3.3930E-04
350.00	3.230	0.001	3.231	631.750	6.0937E-05
400.00	1.390	0.001	1.391	459.840	1.1511E-05
424.50	0.939	0.000	0.939	391.250	5.3637E-06

12.192m AFE

Time seconds	Rad. Eq.			Temperature °C	Pressure Atmos.
	Convective w/cm ²	Radiative w/cm ²	Combined w/cm ²		
0.00	1.519	0.003	1.522	476.550	1.2784E-05
20.00	6.018	0.058	6.076	786.530	2.0546E-04
40.00	20.723	0.708	21.431	1179.000	2.4911E-03
60.00	43.302	50.899	94.201	1829.400	1.1953E-02
70.00	51.690	70.190	121.880	1969.300	1.8445E-02
80.00	56.669	65.757	122.430	1971.800	2.4513E-02

**Table III - Stagnation Point Heating and Pressure for
the Vehicles Aerocapturing at Earth (Continued)**

12.192m AFE (Continued)

Time seconds	Convective w/cm ²	Radiative w/cm ²	Combined w/cm ²	Temperature °C	Rad. Eq. Atmos.	Pressure Atmos.
90.00	58.859	58.484	117.340	1948.100	3.0058E-02	
95.00	59.079	55.065	114.140	1932.800	3.2691E-02	
100.00	59.240	45.467	104.710	1885.700	3.4565E-02	
110.00	53.968	22.861	76.829	1725.000	3.2639E-02	
120.00	45.790	13.208	58.997	1597.300	2.8333E-02	
140.00	34.076	2.397	36.473	1385.400	2.0816E-02	
160.00	26.831	1.086	27.917	1278.200	1.6256E-02	
180.00	21.966	0.520	22.486	1196.500	1.2856E-02	
200.00	17.458	0.313	17.771	1112.600	9.2028E-03	
250.00	8.544	0.073	8.616	883.200	2.6314E-03	
300.00	3.836	0.015	3.851	672.350	5.5246E-04	
350.00	1.680	0.002	1.682	495.520	1.1372E-04	
400.00	0.801	0.001	0.802	365.710	2.5984E-05	

4.37m Apollo CM

Time seconds	Convective w/cm ²	Radiative w/cm ²	Combined w/cm ²	Temperature °C	Rad. Eq. Atmos.	Pressure Atmos.
0.00	1.270	0.001	1.271	443.560	1.0281E-05	
20.00	1.978	0.035	2.013	530.890	2.3975E-04	
40.00	30.063	0.876	30.939	1318.600	6.0949E-03	
60.00	84.209	53.351	137.560	2038.200	4.9806E-02	
65.00	98.554	77.706	176.260	2185.900	6.9429E-02	
70.00	109.970	107.330	217.300	2318.000	9.0786E-02	
74.00	113.490	117.800	231.290	2358.800	1.1155E-01	
80.00	122.680	121.430	244.120	2394.500	1.2928E-01	
84.00	123.250	98.202	221.450	2330.300	1.4232E-01	
94.00	116.550	46.780	163.330	2139.600	1.4550E-01	
104.00	99.349	21.132	120.480	1962.800	1.2254E-01	
154.00	50.230	2.922	53.153	1549.200	5.0456E-02	
204.00	30.971	0.806	31.777	1329.300	2.3936E-02	
304.00	5.941	0.024	5.965	781.670	9.5892E-04	
445.00	0.427	0.000	0.427	272.440	5.2148E-06	

**Table III - Stagnation Point Heating and Pressure for
the Vehicles Aerocapturing at Earth (Continued)**

18.288m x 14.63m Raked Cone

Time seconds	Rad. Eq.			Temperature °C	Pressure Atmos.
	Convective w/cm ²	Radiative w/cm ²	Combined w/cm ²		
0.00	0.463	0.001	0.464	284.220	1.0280E-05
20.00	1.980	0.024	2.005	530.110	1.7198E-04
40.00	11.474	0.036	11.510	978.670	2.9877E-03
60.00	35.216	21.166	56.381	1576.400	2.0706E-02
70.00	42.377	29.326	71.703	1690.900	3.2665E-02
75.00	44.091	27.147	71.237	1687.600	3.6656E-02
80.00	43.671	23.140	66.811	1656.400	3.8321E-02
100.00	36.294	4.611	40.905	1432.600	2.7003E-02
140.00	21.188	0.596	21.785	1185.300	1.3131E-02
200.00	12.109	0.257	12.366	986.440	7.5184E-03
300.00	2.630	0.047	2.677	590.330	1.7334E-03
400.00	0.964	0.010	0.973	397.330	3.5549E-04
500.00	0.245	0.001	0.247	202.280	5.7362E-05
600.00	0.086	0.000	0.086	93.000	8.2826E-06

40° Domed Cylinder (10.67m x 22.86m)

Time seconds	Rad. Eq.			Temperature °C	Pressure Atmos.
	Convective w/cm ²	Radiative w/cm ²	Combined w/cm ²		
0.00	0.560	0.001	0.561	311.440	1.0281E-05
25.00	3.893	0.059	3.952	678.670	3.9319E-04
50.00	32.424	8.841	41.265	1437.600	1.1499E-02
70.00	57.914	53.885	111.800	1921.400	4.5691E-02
80.00	66.993	70.341	137.330	2037.600	6.2668E-02
90.00	70.466	62.158	132.620	2017.000	7.3844E-02
95.00	72.508	54.202	126.710	1991.400	7.9246E-02
110.00	67.526	24.525	92.051	1817.600	7.5729E-02
130.00	56.427	9.096	65.523	1647.600	6.0971E-02
200.00	33.979	1.397	35.376	1373.100	2.8231E-02
300.00	4.869	0.072	4.941	733.110	2.8392E-03
450.00	0.143	0.004	0.147	142.560	1.5326E-05

**Table III - Stagnation Point Heating and Pressure for
the Vehicles Aerocapturing at Earth (Continued)**

55° Domed Cylinder (8.53m x 19.81m)

Time seconds	Convective w/cm ²	Radiative w/cm ²	Combined w/cm ²	Temperature °C	Rad. Eq. Atmos.	Pressure Atmos.
0.00	0.567	0.001	0.569	313.170	1.0280E-05	
20.00	2.603	0.028	2.632	586.440	1.9602E-04	
40.00	17.986	0.594	18.579	1127.400	3.9808E-03	
60.00	48.032	28.486	76.518	1722.900	3.0253E-02	
70.00	62.258	52.319	114.580	1934.900	5.1689E-02	
75.00	67.073	55.723	122.800	1973.500	6.0980E-02	
80.00	68.899	51.218	120.120	1961.100	6.7353E-02	
85.00	69.090	41.685	110.770	1916.400	6.9863E-02	
90.00	67.084	34.626	101.710	1870.100	6.8384E-02	
100.00	60.551	15.503	76.054	1719.900	5.9690E-02	
150.00	40.036	2.179	42.215	1447.200	3.3390E-02	
200.00	27.817	0.590	28.408	1285.000	1.8551E-02	
300.00	3.191	0.044	3.236	632.610	1.7315E-03	
450.00	0.118	0.000	0.118	122.720	1.0128E-05	

57° Domed Cylinder (8.53 x 19.81m)

Time seconds	Convective w/cm ²	Radiative w/cm ²	Combined w/cm ²	Temperature °C	Rad. Eq. Atmos.	Pressure Atmos.
0.00	0.569	0.000	0.569	313.010	1.0280E-05	
20.00	2.420	0.025	2.445	570.830	1.7191E-04	
40.00	14.027	0.430	14.457	1042.900	3.0044E-03	
60.00	42.763	18.896	61.659	1618.100	2.2053E-02	
70.00	53.544	34.784	88.329	1795.900	3.7793E-02	
77.00	59.321	39.074	98.395	1852.400	4.4954E-02	
80.00	60.547	38.030	98.577	1853.400	5.0299E-02	
85.00	60.739	32.730	93.470	1825.300	5.3082E-02	
90.00	59.729	26.602	86.331	1784.100	5.3047E-02	
110.00	51.172	8.378	59.550	1601.700	4.3251E-02	
150.00	38.961	2.037	40.998	1434.600	2.9035E-02	
200.00	27.203	0.580	27.783	1276.400	1.6788E-02	
300.00	5.297	0.079	5.376	754.590	3.0428E-03	
450.00	0.327	0.000	0.327	237.260	6.7642E-05	

**Table IV - Stagnation Point Heating and Pressure for
the Vehicles Aerocapturing at Mars**

12.192m AFE

Time seconds	Convective w/cm ²	Radiative w/cm ²	Combined w/cm ²	Temperature °C	Pressure Atmos.
0.00	0.320	0.000	0.320	234.580	2.9157E-06
20.00	1.858	0.003	1.861	515.240	9.7676E-05
40.00	7.511	0.346	7.857	856.850	1.6196E-03
60.00	19.628	6.202	25.830	1248.400	1.1807E-02
70.00	25.762	11.423	37.185	1393.500	2.1890E-02
80.00	29.839	17.340	47.179	1495.700	3.2905E-02
90.00	31.709	19.501	51.210	1532.300	4.3164E-02
100.00	31.255	17.112	48.367	1506.700	5.0177E-02
110.00	28.900	10.649	39.549	1419.300	5.2589E-02
120.00	25.394	2.514	27.908	1278.100	5.0982E-02
140.00	18.162	0.012	18.174	1120.400	4.2688E-02
160.00	13.201	0.003	13.204	1013.400	3.4046E-02
180.00	9.801	0.001	9.802	921.090	2.6792E-02
200.00	7.171	0.000	7.171	831.350	1.9046E-02
250.00	3.902	0.000	3.902	675.470	8.7737E-03
300.00	2.429	0.000	2.429	569.460	4.2243E-03
400.00	1.099	0.000	1.099	417.900	9.9772E-04
500.00	0.507	0.000	0.507	296.540	2.1589E-04

6 km/s Biconic (0.3048m nose Radius)

Time seconds	Convective w/cm ²	Radiative w/cm ²	Combined w/cm ²	Temperature °C	Pressure Atmos.
0.00	0.611	< 0.01	0.611	323.560	1.6054E-06
20.00	2.135		2.135	542.670	1.9764E-05
40.00	6.360		6.360	798.670	1.8291E-04
60.00	16.018		16.018	1077.100	1.2077E-03
70.00	23.638		23.638	1215.000	2.6930E-03
80.00	32.849		32.849	1342.600	5.3451E-03
90.00	42.863		42.863	1453.700	9.4104E-03
100.00	52.314		52.314	1541.900	1.4595E-02
110.00	59.311		59.311	1599.800	1.9664E-02
120.00	62.537		62.537	1624.800	2.2964E-02
130.00	62.488		62.488	1624.400	2.4084E-02
150.00	60.724		60.724	1610.800	2.5128E-02
170.00	57.915	< 0.01	57.915	1588.700	2.5317E-02

**Table IV - Stagnation Point Heating and Pressure for
the Vehicles Aerocapturing at Mars (Continued)**

6 km/s Biconic (0.3048m nose Radius) (Continued)

Time seconds	Convective		Combined w/cm ²	Temperature °C	Pressure Atmos.
	Radiative w/cm ²	Rad. Eq.			
200.00	52.748	< 0.01	52.748	1545.700	2.4474E-02
300.00	36.475		36.475	1385.400	1.8761E-02
400.00	25.644		25.644	1245.600	1.3642E-02
600.00	14.508		14.508	1044.100	7.5309E-03
800.00	6.081	< 0.01	6.081	786.780	1.6411E-03

6 km/s Biconic (0.6096m nose Radius)

Time seconds	Convective		Combined w/cm ²	Temperature °C	Pressure Atmos.
	Radiative w/cm ²	Rad. Eq. w/cm ²			
0.00	0.431	< 0.01	0.431	274.060	1.6054E-06
20.00	1.509		1.509	475.000	1.9764E-05
40.00	4.496		4.496	709.720	1.8291E-04
60.00	11.326		11.326	965.000	1.2077E-03
70.00	16.715		16.715	1091.500	2.6930E-03
80.00	23.228		23.228	1208.500	5.3451E-03
90.00	30.308		30.308	1310.400	9.4104E-03
100.00	36.992		36.992	1391.300	1.4595E-02
110.00	41.939		41.939	1444.400	1.9664E-02
120.00	44.220		44.220	1467.300	2.2964E-02
130.00	44.186		44.186	1466.900	2.4084E-02
150.00	42.938		42.938	1454.500	2.5128E-02
170.00	40.953		40.953	1434.200	2.5317E-02
200.00	37.298		37.298	1394.700	2.4474E-02
300.00	25.793		25.793	1247.800	1.8761E-02
400.00	18.133		18.133	1119.600	1.3642E-02
600.00	10.259		10.259	934.780	7.5309E-03
800.00	4.300	< 0.01	4.300	698.780	1.6411E-03

8 km/s Biconic (0.6096m nose Radius)

Time seconds	Convective		Combined w/cm ²	Temperature °C	Pressure Atmos.
	Radiative w/cm ²	Rad. Eq. w/cm ²			
0.00	1.220	0.113	1.334	452.200	2.9159E-06
20.00	7.048	0.340	7.388	839.600	1.1236E-04
40.00	32.560	0.794	33.355	1348.800	2.1607E-03

**Table IV - Stagnation Point Heating and Pressure for
the Vehicles Aerocapturing at Mars (Continued)**

8 km/s Biconic (0.6096m nose Radius) (Continued)

Time seconds	Convective w/cm ²	Radiative w/cm ²	Combined w/cm ²	Temperature °C	Pressure Atmos.
60.00	92.028	1.657	93.685	1826.500	1.7623E-02
80.00	149.120	6.582	155.930	2111.700	4.7762E-02
90.00	158.430	8.228	166.660	2151.700	5.4395E-02
100.00	162.180	8.512	170.690	2166.300	5.7846E-02
110.00	161.610	8.852	170.460	2165.400	5.9118E-02
120.00	157.860	7.944	165.810	2148.600	5.8731E-02
150.00	138.800	5.402	144.200	2065.600	5.3110E-02
200.00	107.740	1.555	109.290	1909.000	4.2223E-02
250.00	85.253	0.681	85.934	1781.700	3.3730E-02
300.00	69.331	0.340	69.671	1676.700	2.7339E-02
350.00	57.573	0.113	57.687	1586.800	2.2456E-02
400.00	48.528	0.011	48.562	1508.500	1.8654E-02
500.00	35.772	0.001	35.795	1377.700	1.3221E-02
600.00	27.487	0.000	27.487	1272.200	9.6187E-03
700.00	21.960		21.960	1187.900	7.1491E-03
800.00	15.832		15.832	1073.100	3.5832E-03
900.00	8.732		8.732	887.070	1.1999E-03
1000.00	4.709		4.709	721.100	3.8043E-04

10 km/s Biconic (0.6096m nose Radius)

Time seconds	Convective w/cm ²	Radiative w/cm ²	Combined w/cm ²	Temperature °C	Pressure Atmos.
0.00	2.077		2.077	537.110	4.6141E-06
10.00	6.885		6.885	820.170	5.1696E-05
20.00	20.144		20.144	1156.700	4.4991E-04
30.00	49.966	0.000	49.966	1521.200	2.8609E-03
40.00	102.360	1.021	103.390	1878.900	1.2802E-02
50.00	158.890	8.625	167.460	2154.600	3.7478E-02
60.00	214.840	16.115	230.950	2357.800	6.9265E-02
70.00	236.060	26.897	263.000	2444.700	9.3705E-02
80.00	236.970	34.160	271.070	2465.300	1.0621E-01
90.00	224.250	33.139	257.360	2430.000	1.0660E-01
100.00	207.000	29.621	236.650	2373.900	1.0137E-01
110.00	191.170	25.649	216.790	2316.500	9.5009E-02
120.00	175.340	22.471	197.850	2258.000	8.8982E-02
140.00	150.370	16.342	166.690	2151.800	7.8486E-02

Table IV - Stagnation Point Heating and Pressure for the Vehicles Aerocapturing at Mars (Continued)

10 km/s Biconic (0.6096m nose Radius)

Time seconds	Convective w/cm ²	Radiative w/cm ²	Combined w/cm ²	Temperature °C	Pressure Atmos.
150.00	140.240	13.165	153.450	2102.200	7.3899E-02
170.00	119.960	9.533	129.490	2003.500	6.5803E-02
190.00	105.020	5.901	110.870	1916.800	5.8901E-02
200.00	97.555	4.880	102.470	1874.100	5.5827E-02
250.00	70.193	0.227	70.455	1682.200	4.3341E-02
300.00	51.797	0.000	51.797	1537.400	3.4405E-02
350.00	40.005		40.005	1424.200	2.7798E-02
400.00	31.743		31.743	1328.800	2.2783E-02
500.00	21.291		21.291	1176.600	1.5821E-02
600.00	15.242		15.242	1060.400	1.1341E-02
700.00	11.474		11.474	969.060	8.3309E-03
800.00	8.785		8.785	888.830	5.9730E-03
1000.00	2.871		2.871	605.440	6.7961E-04

Table IV - Stagnation Point Heating And Pressure For The Vehicles Aerocapturing At Mars (Continued)

12 km/s Biconic (0.6096m nose Radius)

Time seconds	Convective w/cm ²	Radiative w/cm ²	Combined w/cm ²	Temperature °C	Pressure Atmos.
0.00	3.995	0.000	3.995	681.060	6.7006E-06
10.00	18.136	0.000	18.136	1119.700	1.4316E-04
19.00	60.762	0.000	60.762	1611.200	
20.00	65.495	0.681	66.176	1651.800	1.9784E-03
30.00	177.380	24.060	201.400	2269.300	1.6934E-02
40.00	343.530	173.410	516.940	2944.900	7.5455E-02
50.00	455.660	338.650	794.310	3309.700	1.5669E-01
60.00	444.990	260.230	705.220	3204.700	1.8156E-01
70.00	386.660	128.810	515.470	2942.600	1.6431E-01
80.00	335.700	99.530	435.250	2809.400	1.4573E-01
90.00	299.160	70.250	369.440	2685.700	1.3380E-01
100.00	268.520	40.970	309.530	2557.600	1.2461E-01
120.00	224.940	33.820	258.700	2433.500	1.0821E-01
140.00	189.190	25.649	214.860	2310.700	9.4434E-02
150.00	175.870	21.676	197.510	2256.900	8.8478E-02
170.00	149.240	16.229	165.480	2147.400	7.8077E-02

**Table IV - Stagnation Point Heating and Pressure for
the Vehicles Aerocapturing at Mars (Continued)**

12 km/s Biconic (0.6096m nose Radius) (Continued)

Time seconds	Convective w/cm ²	Radiative w/cm ²	Combined w/cm ²	Temperature °C	Pressure Atmos.
190.00	129.340	10.895	140.190	2049.200	6.9328E-02
200.00	119.390	9.420	128.810	2000.500	6.5466E-02
250.00	85.162	2.270	87.409	1790.400	5.0045E-02
251.00	84.686	0.000	84.686	1774.200	
300.00	61.477		61.477	1616.700	3.9216E-02
350.00	46.417		46.417	1488.500	3.1364E-02
400.00	36.305		36.305	1383.600	2.5493E-02
500.00	23.810		23.810	1217.700	1.7480E-02
600.00	16.762		16.762	1092.500	1.2423E-02
700.00	12.461		12.461	994.940	9.0620E-03
800.00	9.518		9.518	912.330	6.7468E-03

Table V - Material Temperature Limits for TPS Materials

TPS Material	Temperature Limit °C
AVCO-5026-H/CG	No upper limit assumed
New Advanced Carbon/Carbon	2094
Advanced Carbon/Carbon	1649
Cerachrome	1483
RFC	1927
FRCI-12	1483
LI-900	1371
RTV-560	288
HTP-6	1483
NOMEX felt	444
FRSI (C-9 coated NOMEX)	371
SIP (RTV-560/NOMEX/RTV-560)	288

Table VI - Typical Benefits of Aerobraking

These vehicles provide from 17% to 85% increase in payload

Vehicle Class	Δ Payload
AFE	
Mars Entry	84 - 85 %
Mars Return	68 - 82 %
Lunar Return	76 - 77 %
Biconic/Domed Cyl	
Mars Entry	55 - 80 %
Lunar Return	57 - 78 %
Apollo	
SRC Mars Return	17 - 50 %
Lunar Return	65 - 67 %

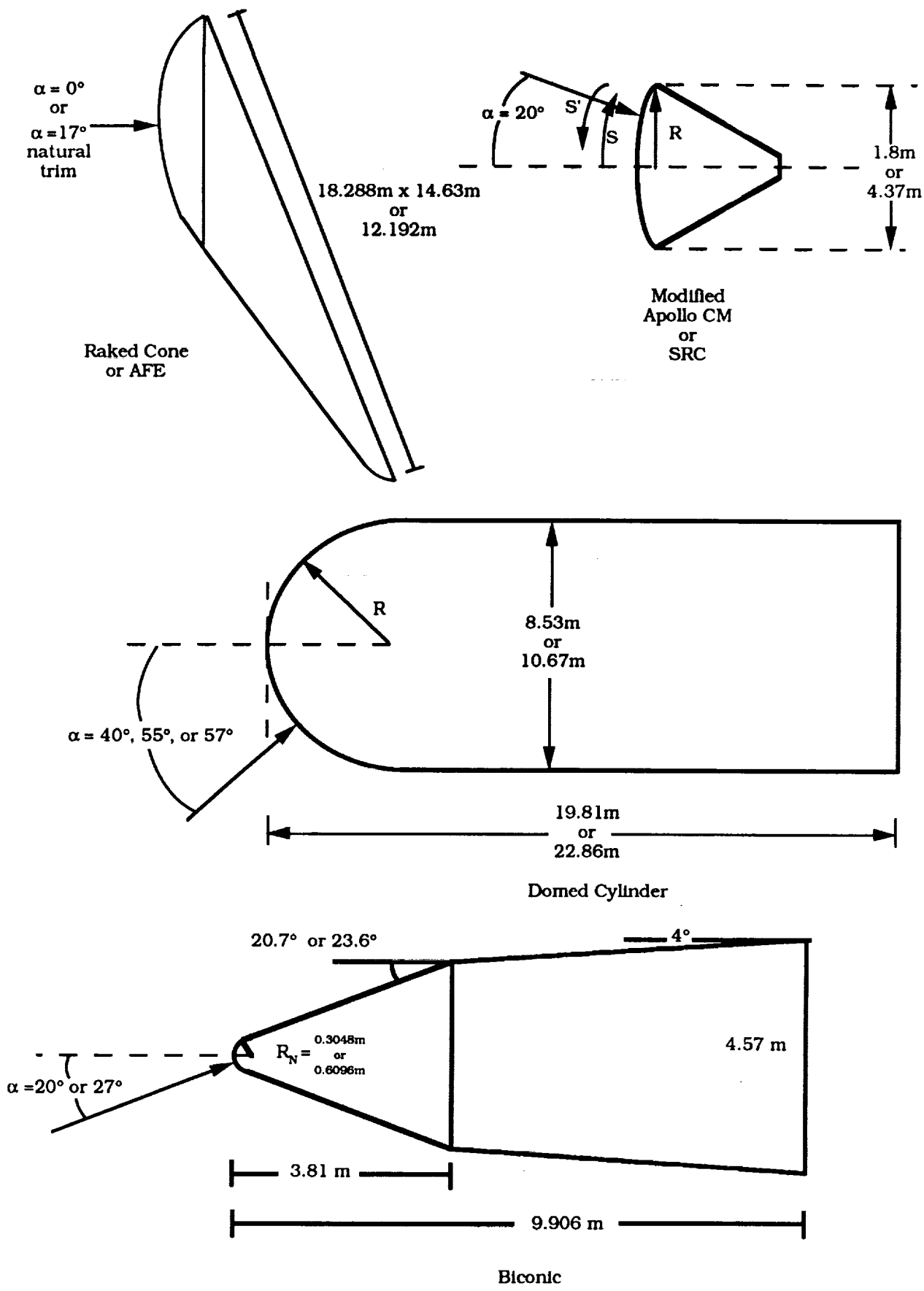


Fig. 1 Sketch of the Vehicles Analyzed for Aerobraking at Mars and Earth.

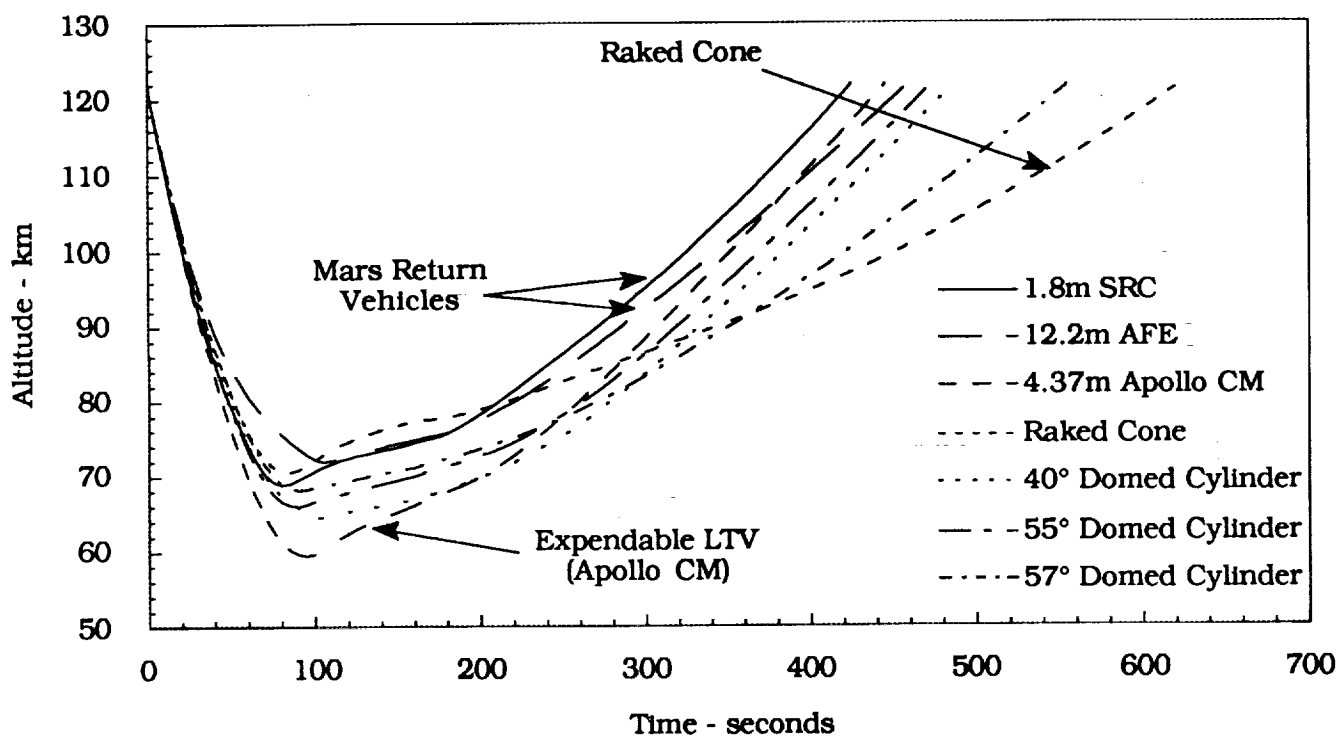


Fig. 2 Altitude vs. Time for the Earth Aerocapture Trajectories.

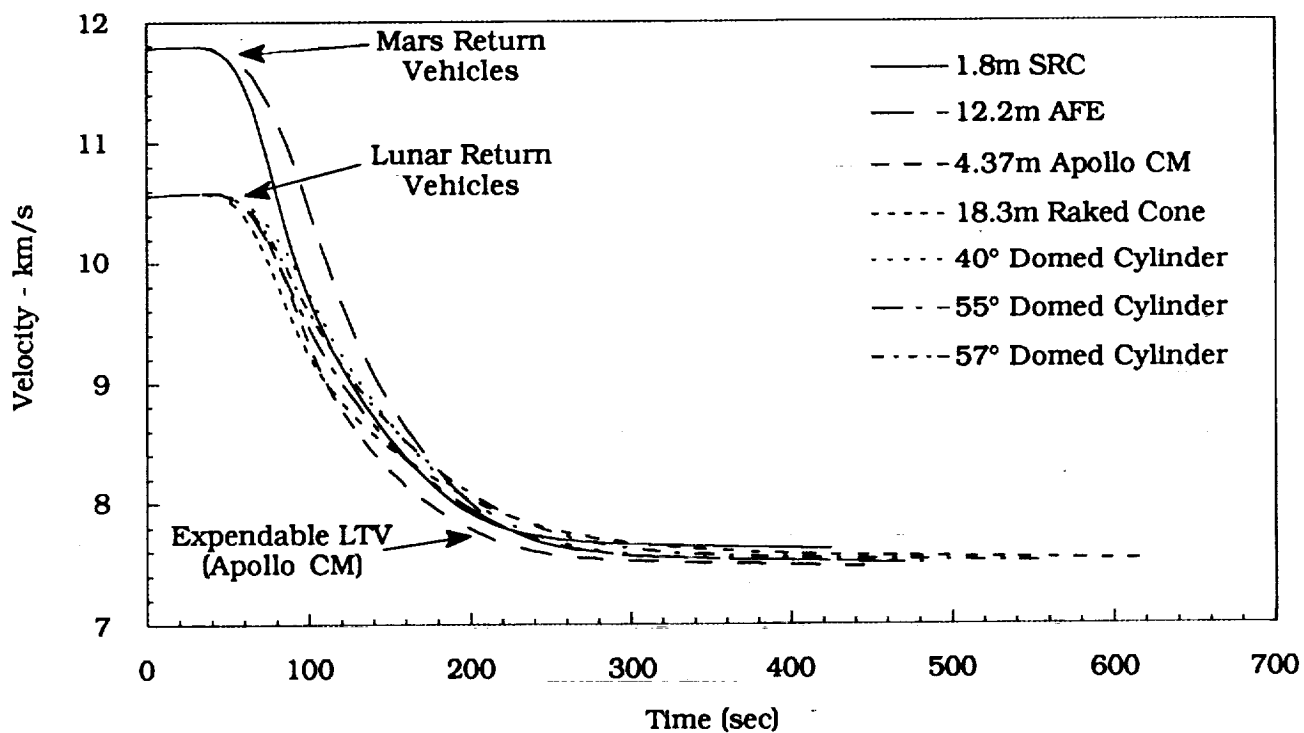


Fig. 3 Velocity vs. Time for the Earth Aerocapture Trajectories.

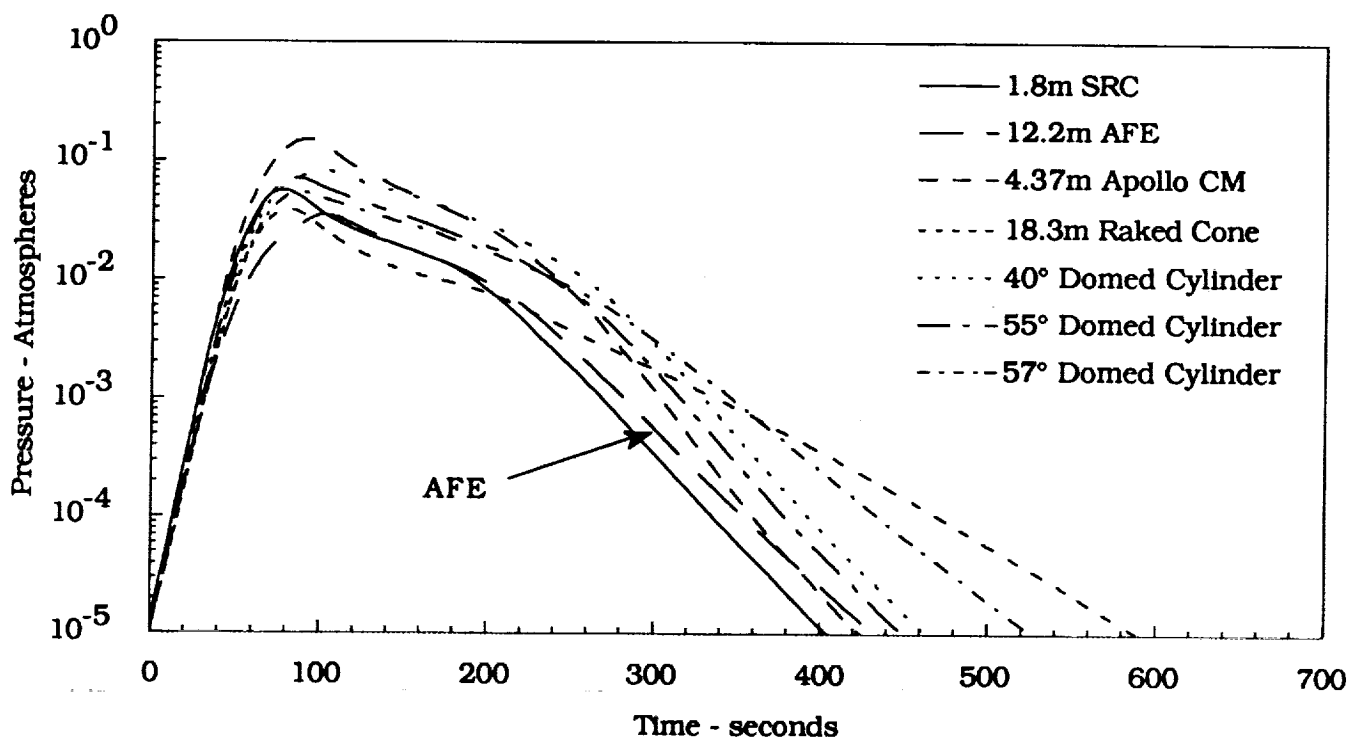


Fig. 4 Pressure vs. Time for the Earth Aerocapture Trajectories.

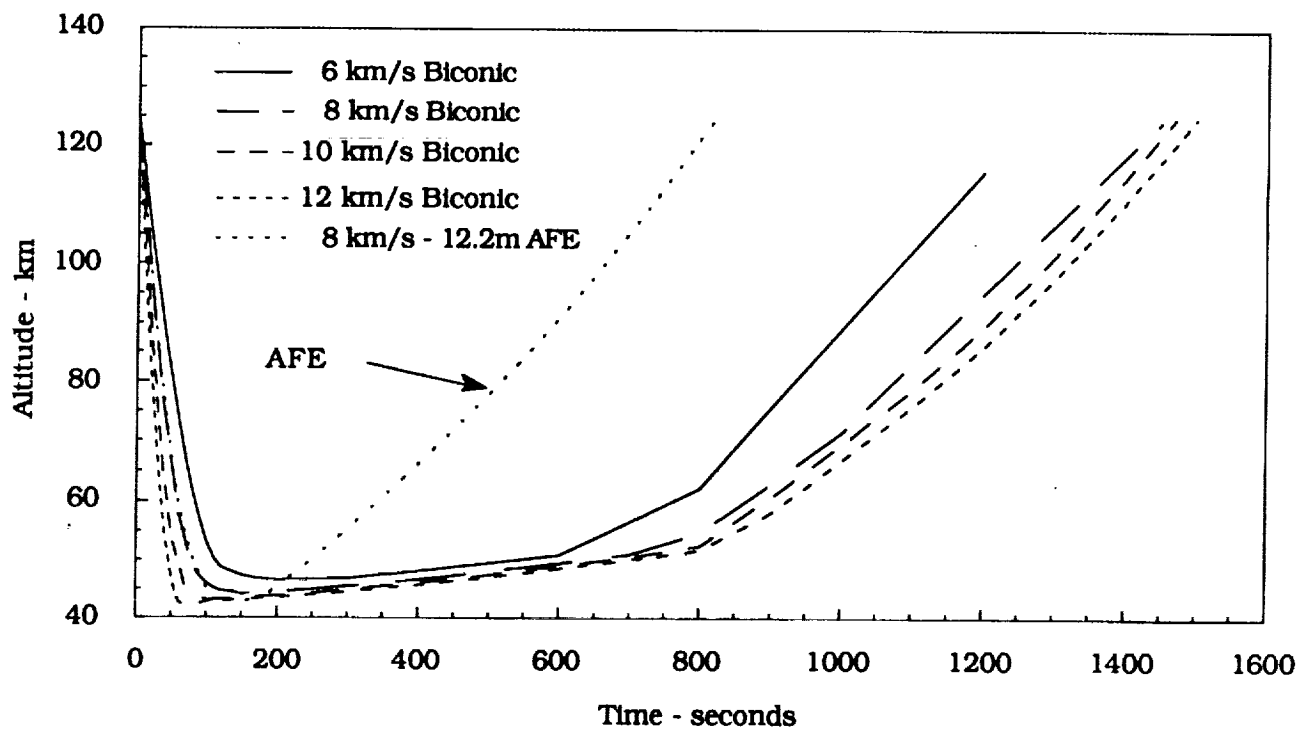


Fig. 5 Altitude vs. Time for the Mars Aerocapture Trajectories.

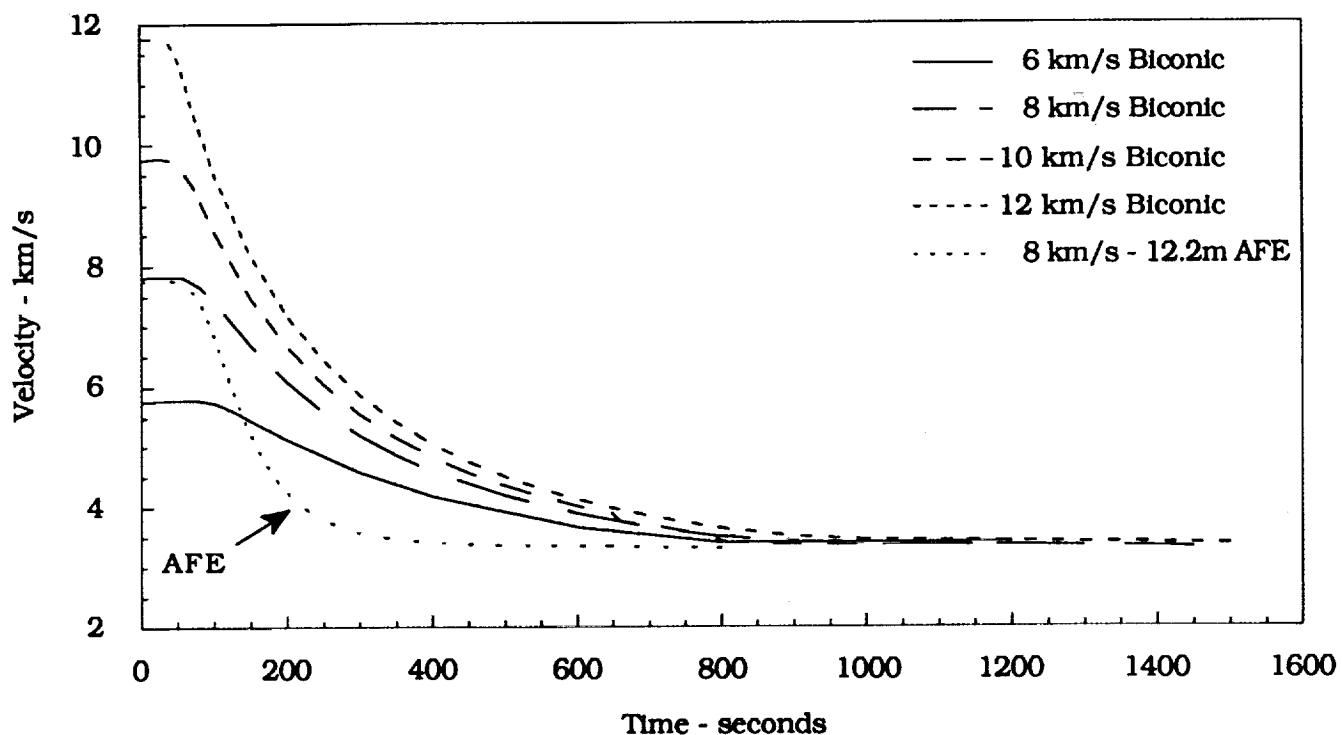


Fig. 6 Velocity vs. Time for the Mars Aerocapture Trajectories.

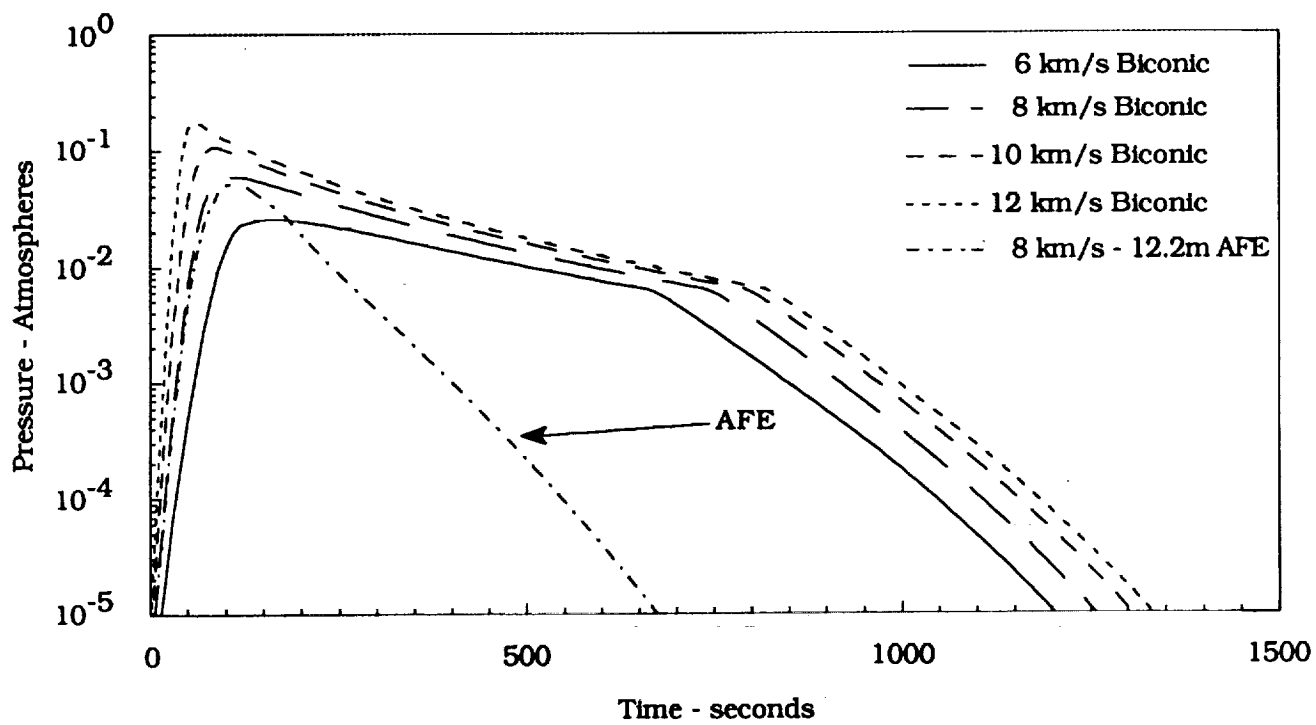


Fig. 7 Pressure vs. Time for the Mars Aerocapture Trajectories.

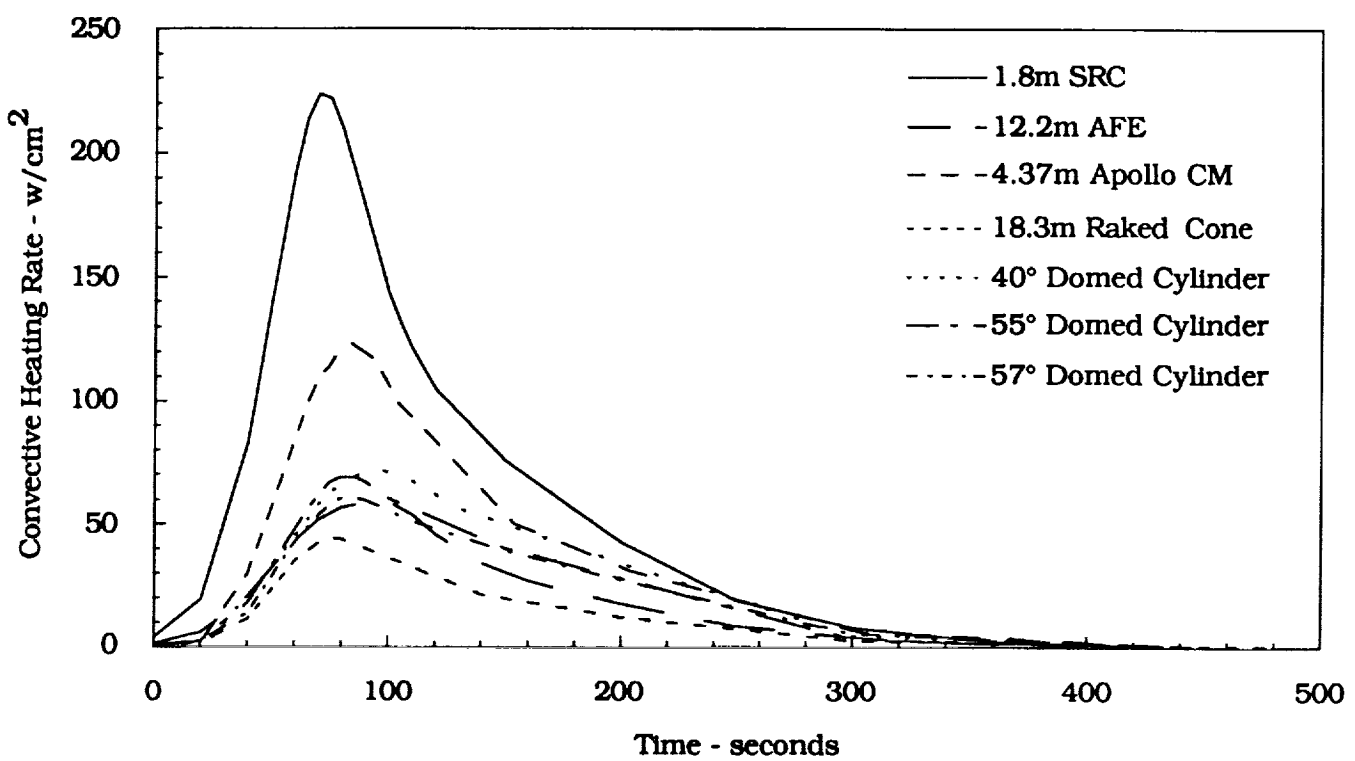


Fig. 8 Convective Heating Rate for the Earth Aerocapture Trajectories.

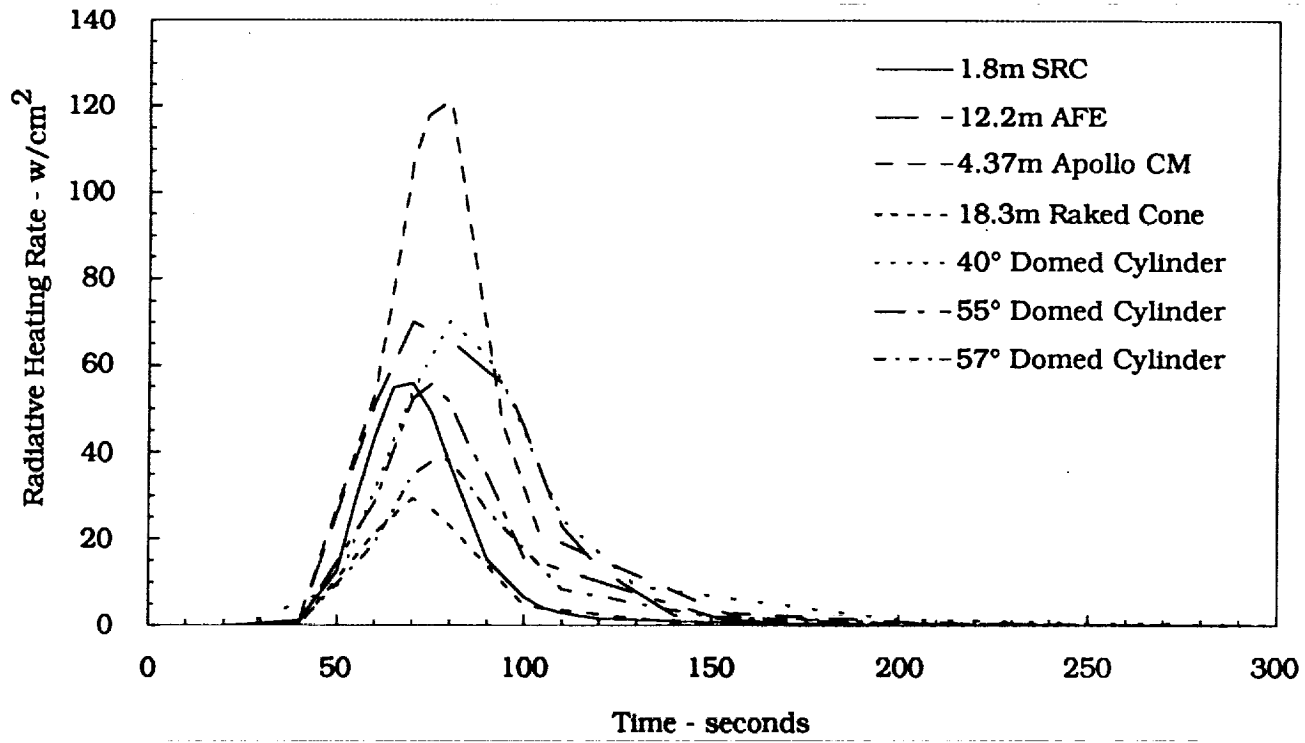


Fig. 9 Radiative Heating Rate for the Earth Aerocapture Trajectories.

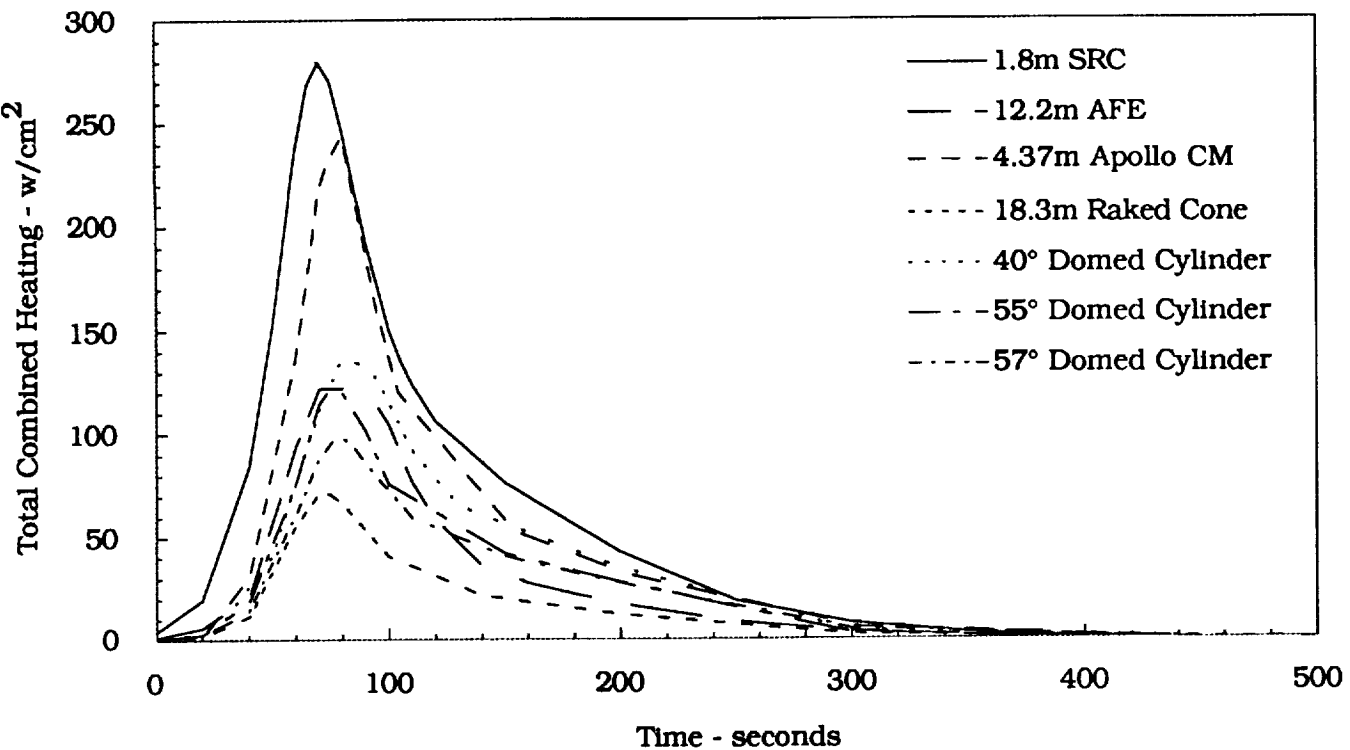


Fig. 10 Combined Heating Rates for the Earth Aerocapture Trajectories.

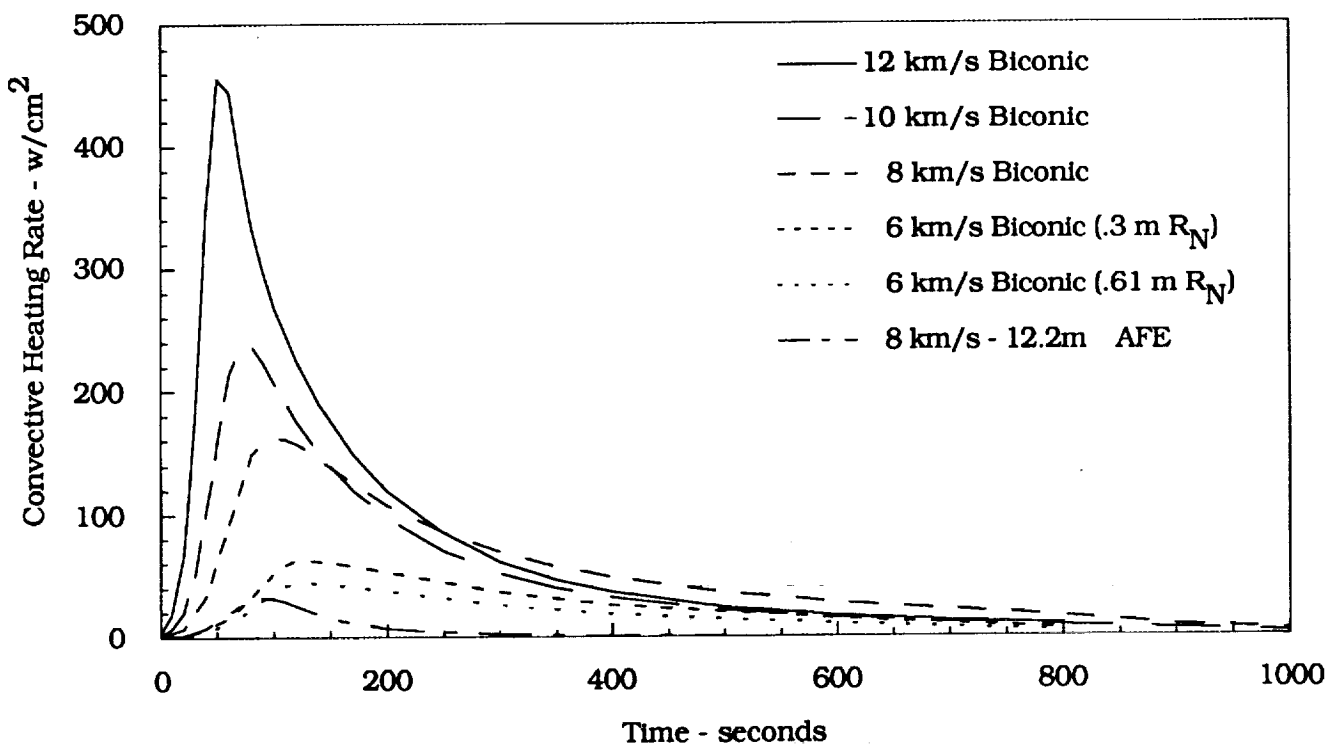


Fig. 11 Convective Heating Rate for the Mars Aerocapture Trajectories.

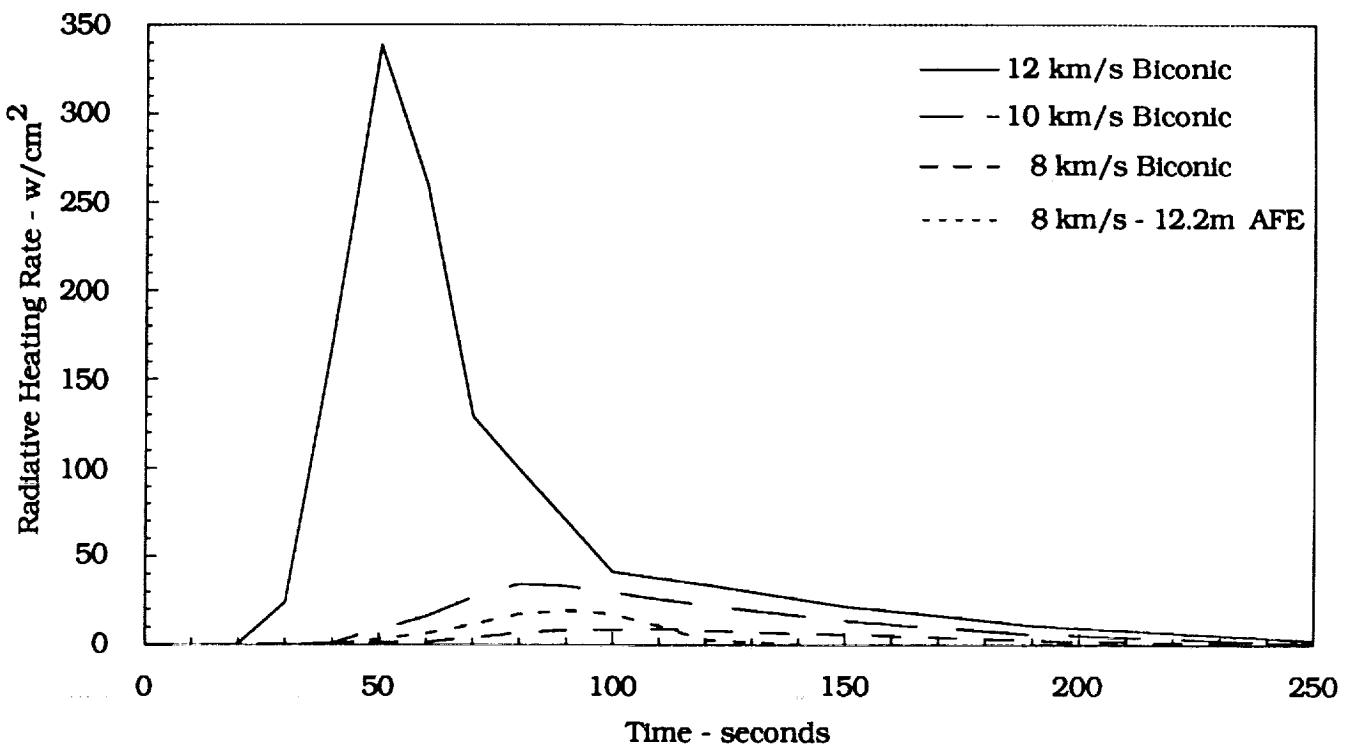


Fig. 12 Radiative Heating Rate for the Mars Aerocapture Trajectories.

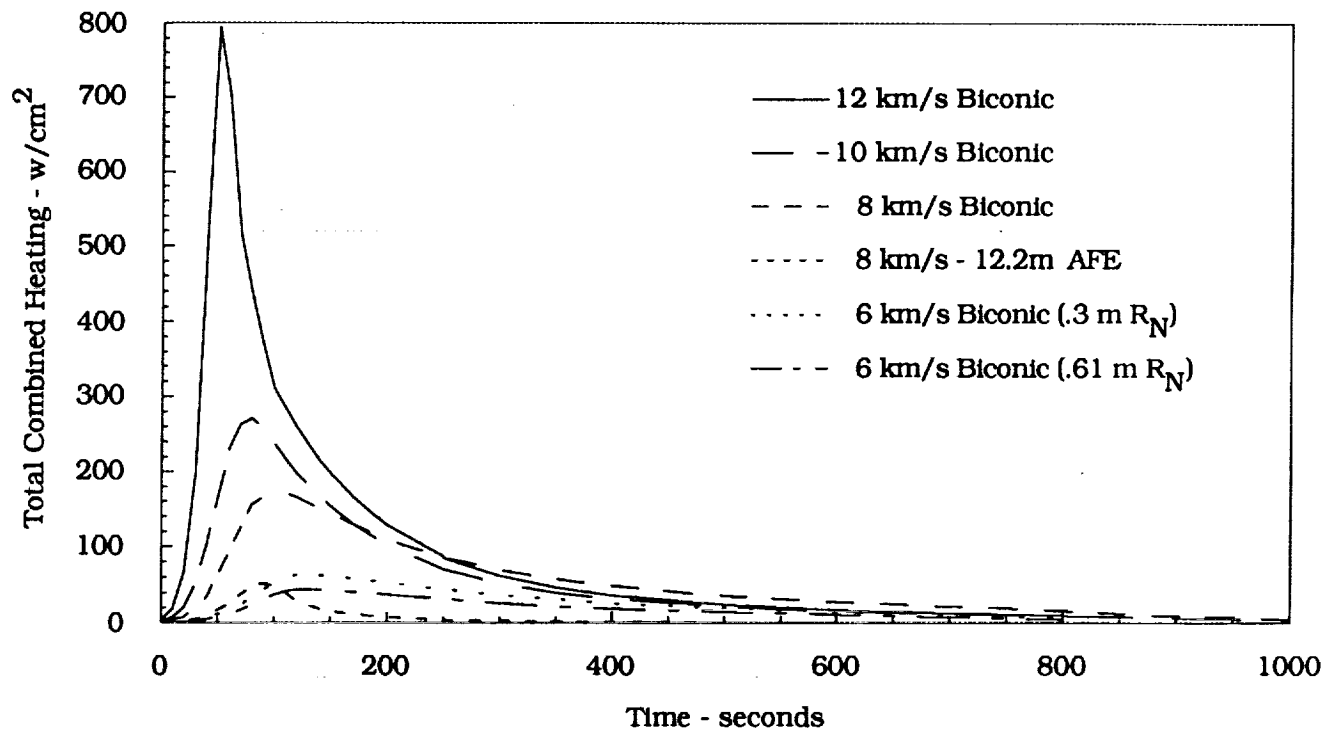


Fig. 13 Combined Heating Rates for the Mars Aerocapture Trajectories.

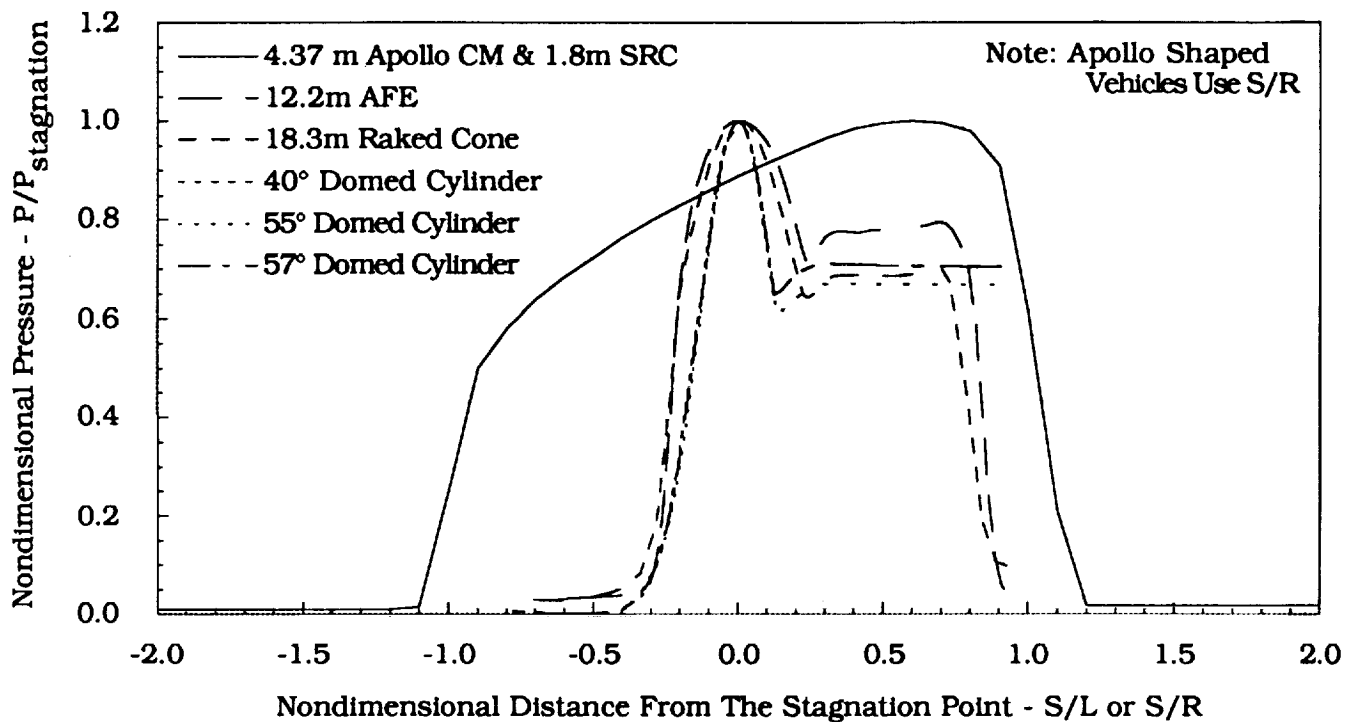


Fig. 14 Pressure Distributions for the Earth Aerocapture Vehicles.

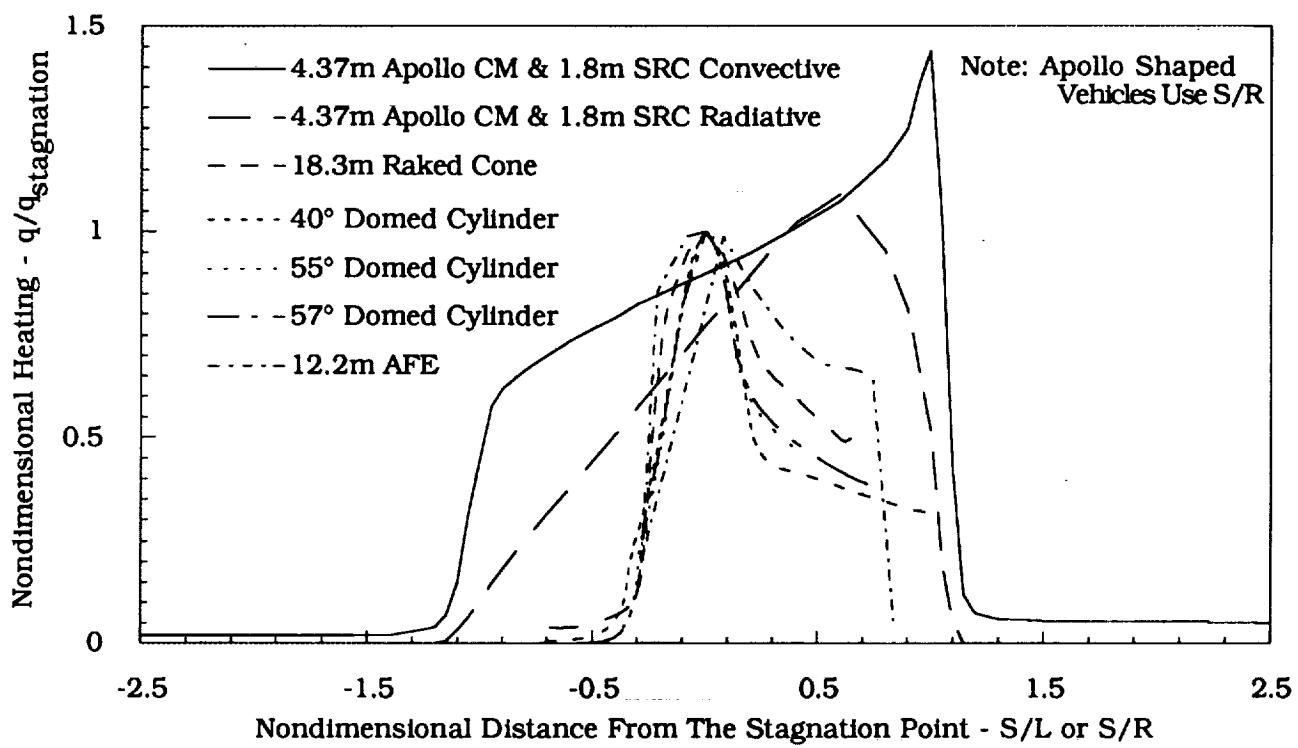


Fig. 15 Heating Distributions For The Earth Aerocapture Vehicles.

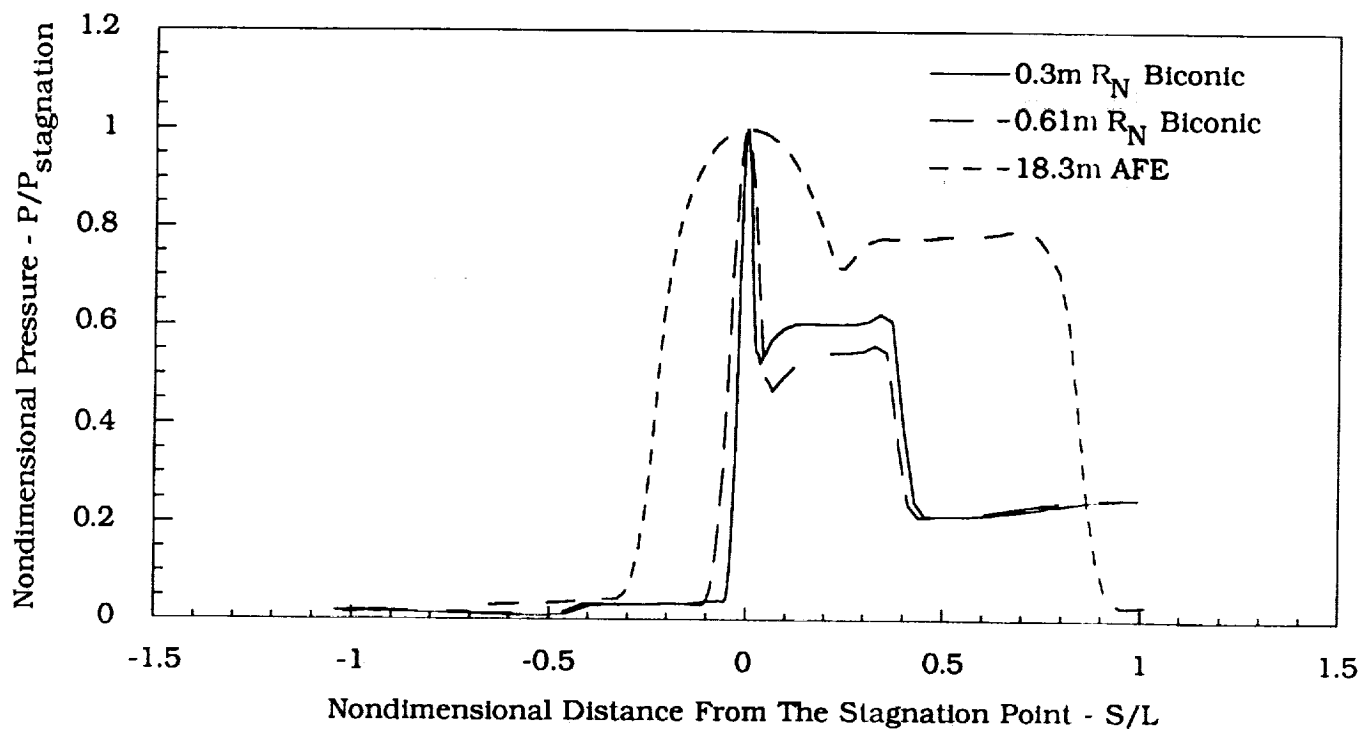


Fig. 16 Pressure Distribution for the Mars Aerocapture Vehicles.

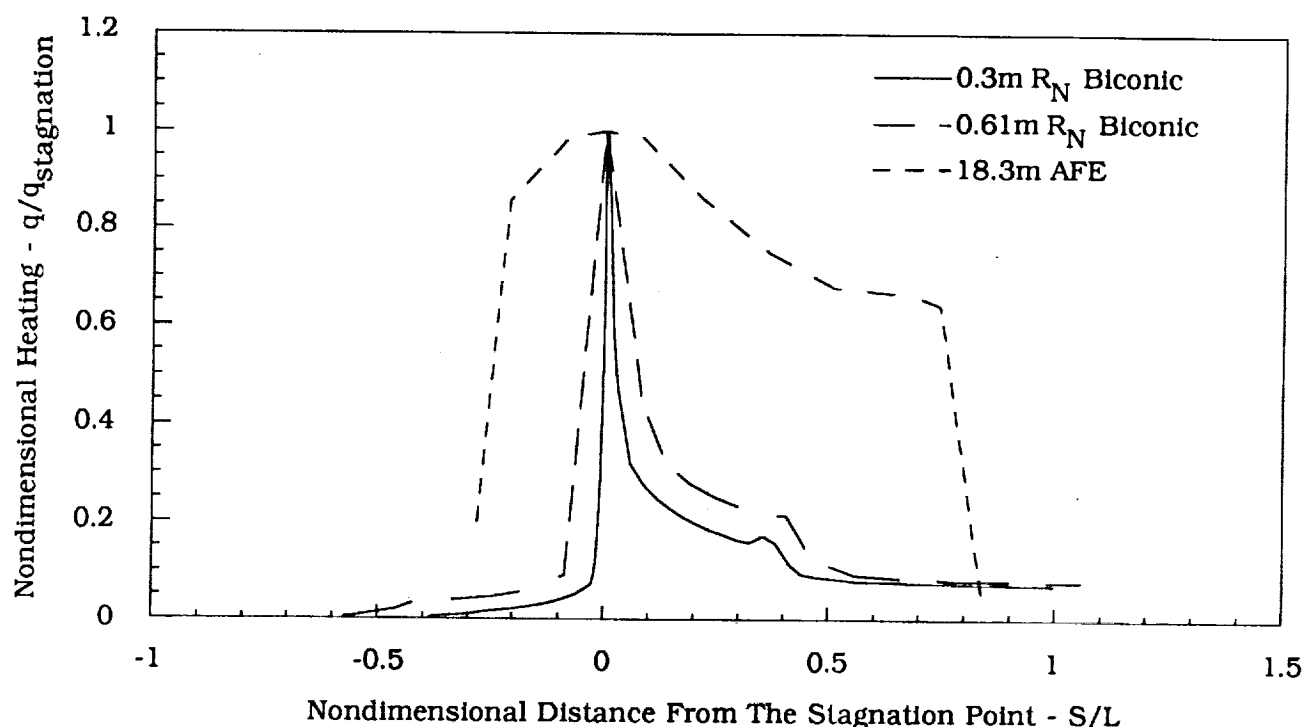


Fig. 17 Heating Distribution for the Mars Aerocapture Vehicles.

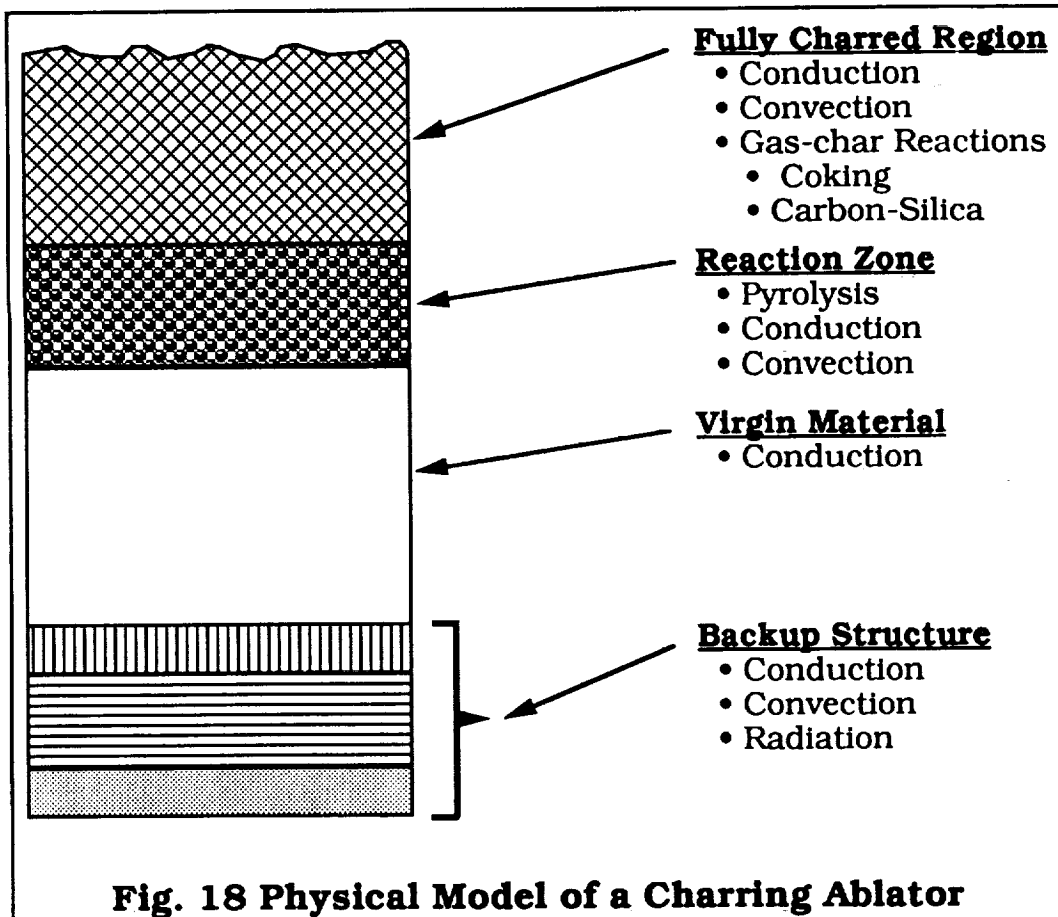


Fig. 18 Physical Model of a Charring Ablator

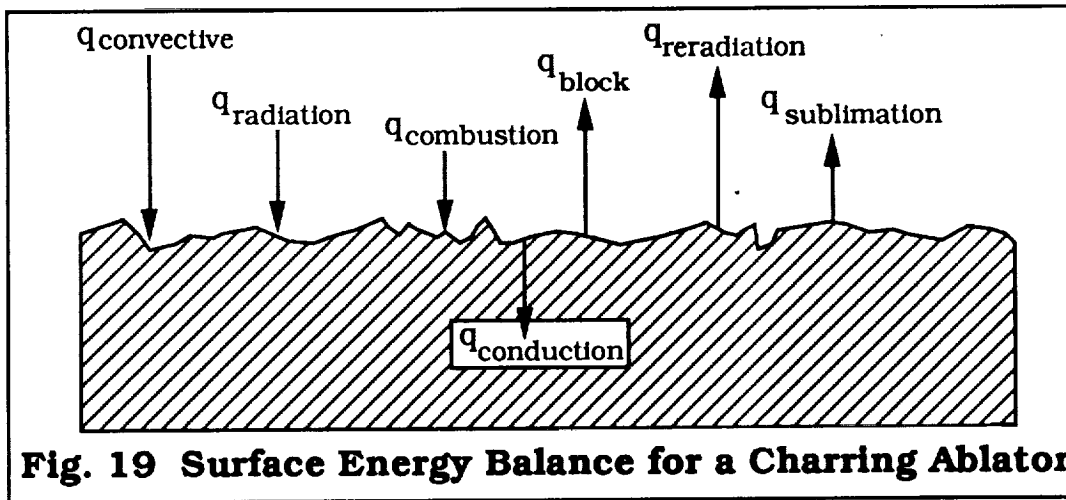


Fig. 19 Surface Energy Balance for a Charring Ablator

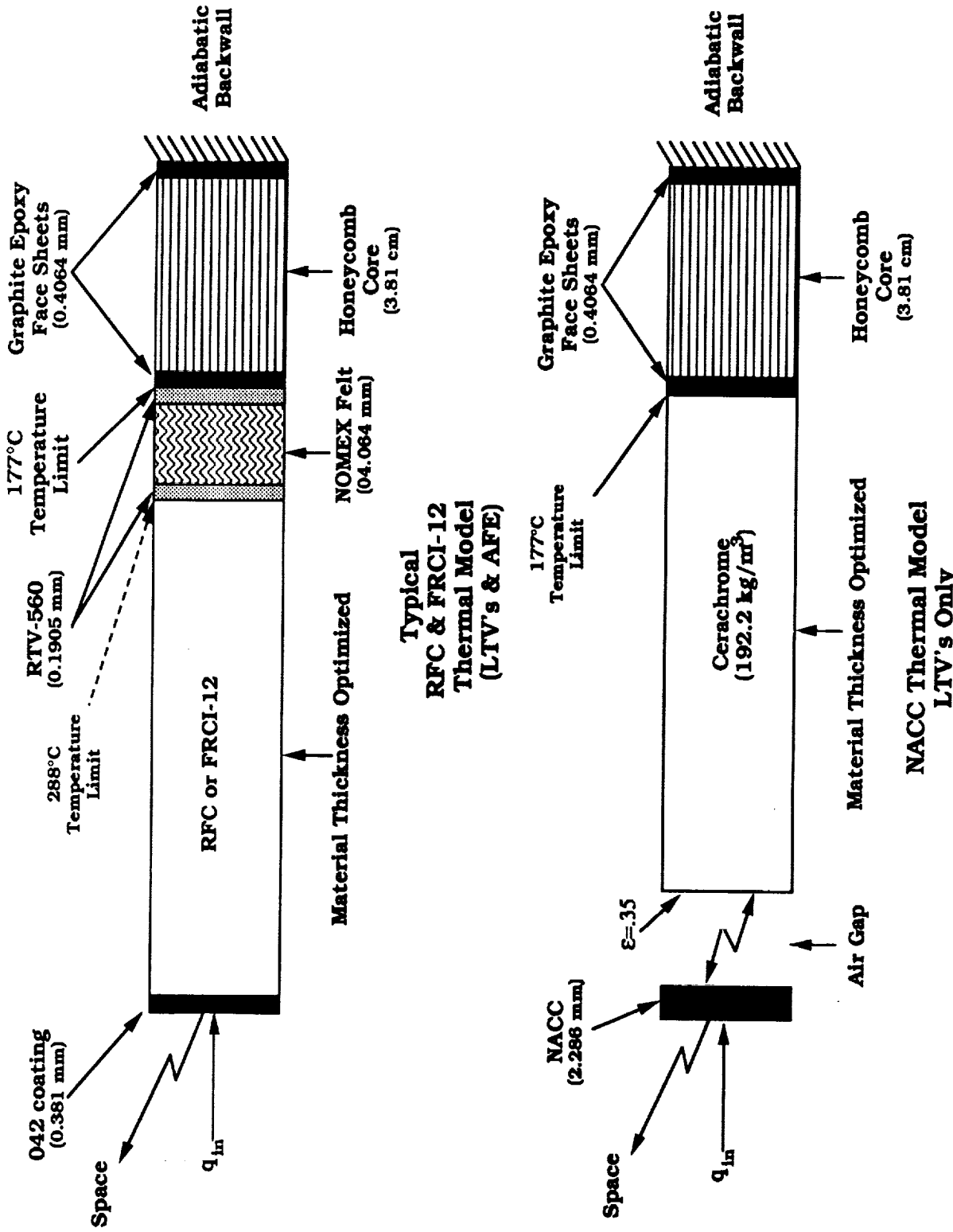
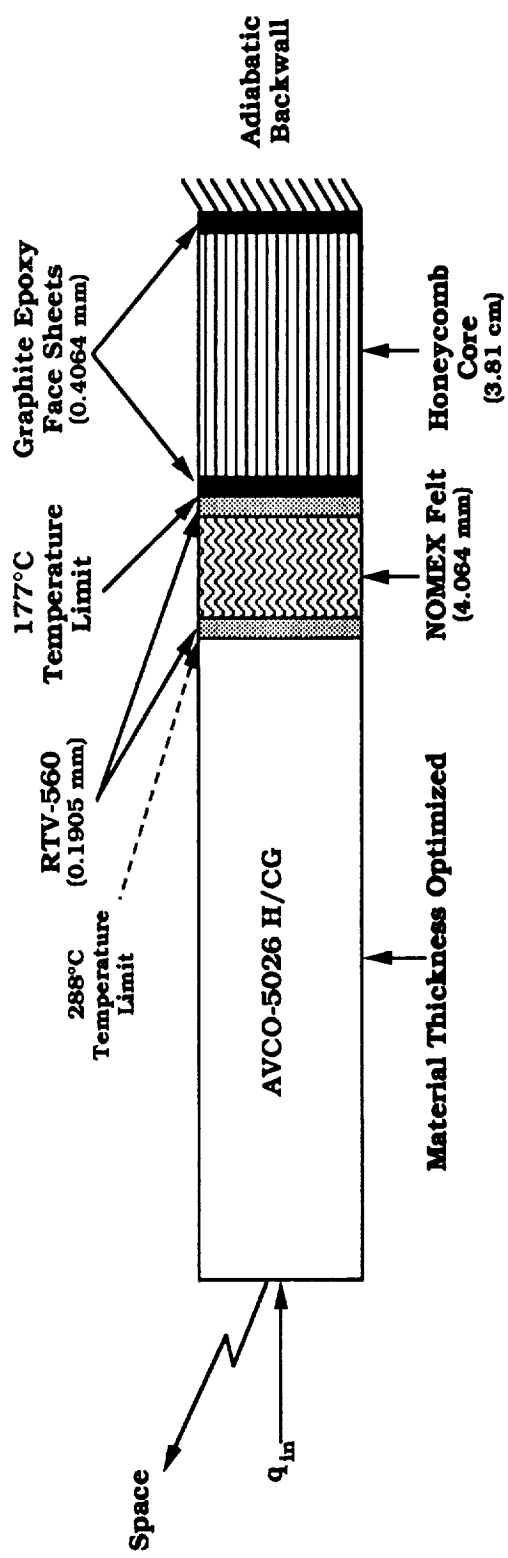
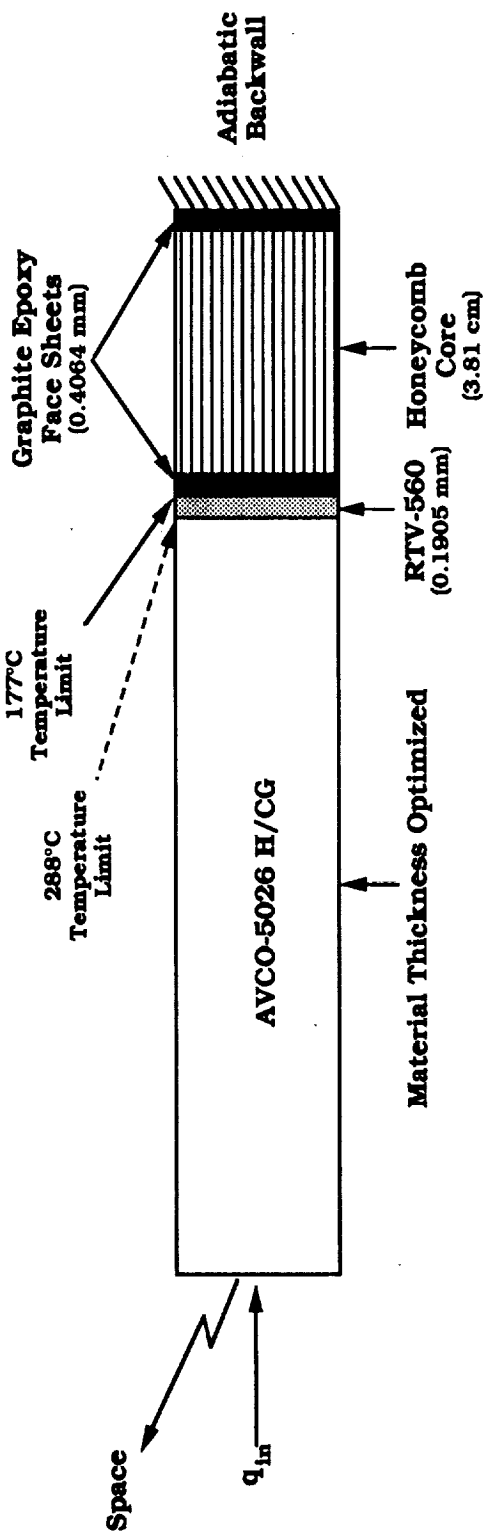


Fig. 20 Sketch of the Reusable Thermal Models.



Thermal Model of the Ablator with SIP



Thermal Model of the Ablator without SIP

Fig. 21 Sketch of the Ablative Thermal Models.

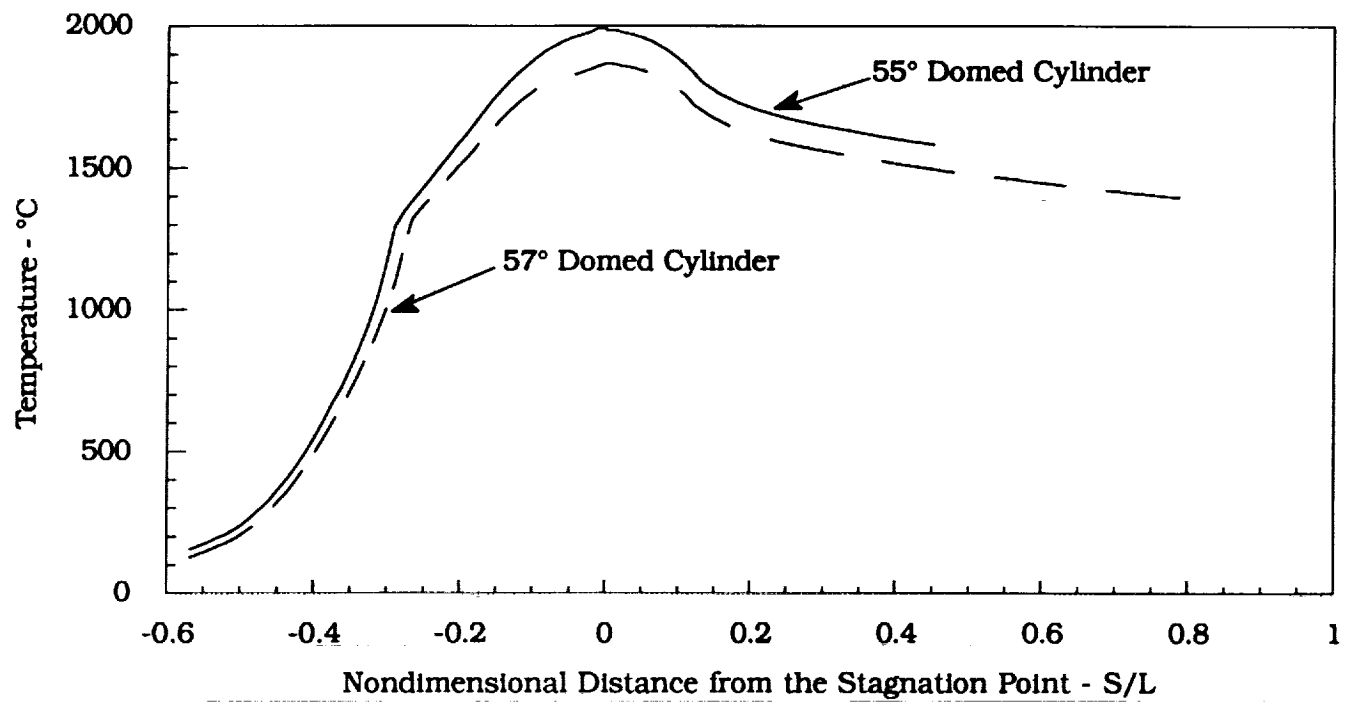


Fig. 22 Radiation Equilibrium Temperature vs. S/L for Two Domed Cylinder Vehicles Entering at $\alpha = 55^\circ$ and 57° .

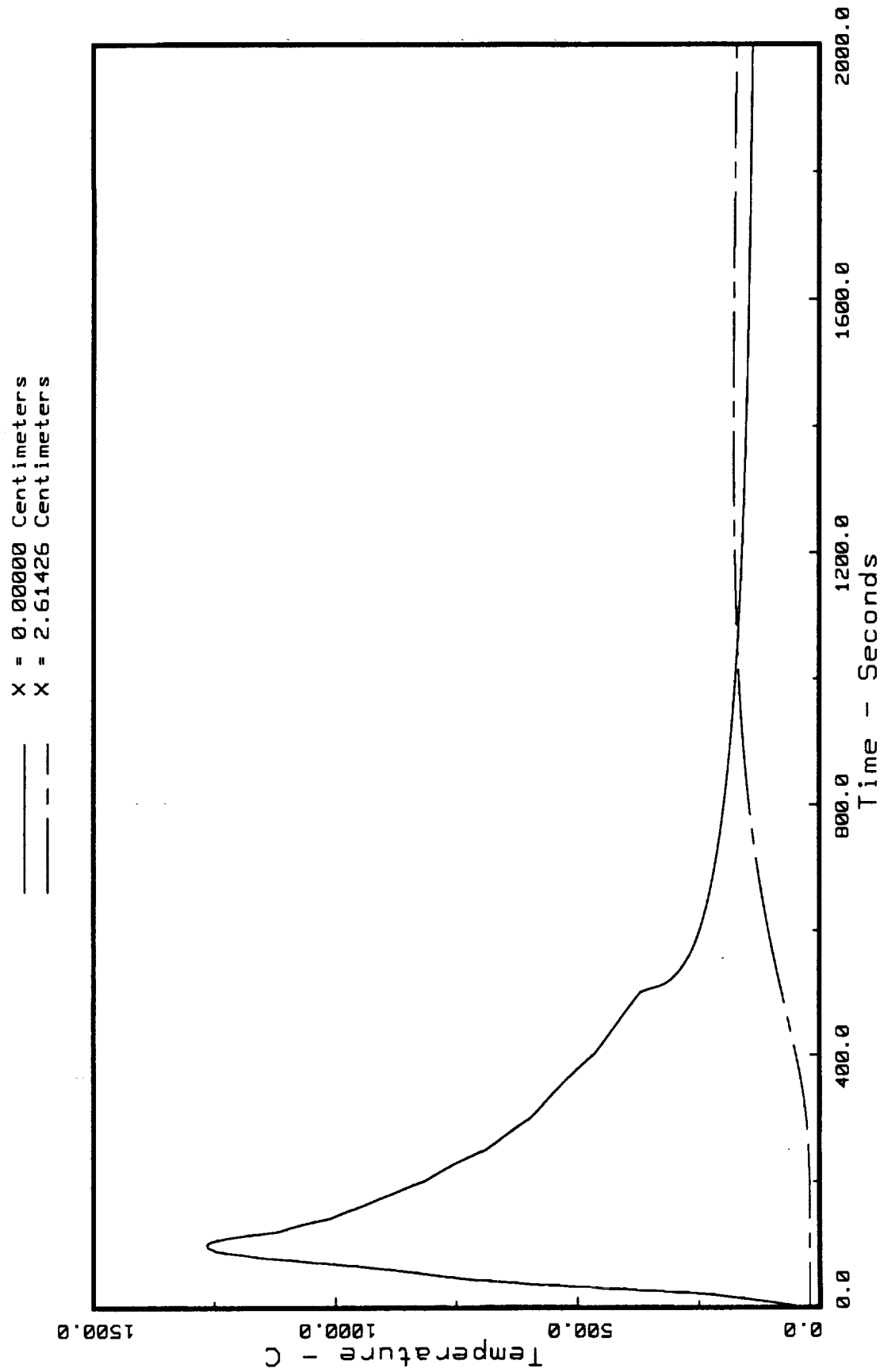


Fig. 23 Mars Aerocapture for the 12.192m AFE - Temperature History of Ablator Surface and Graphite Epoxy Backwall for the First 2000 Seconds at the Stagnation Point

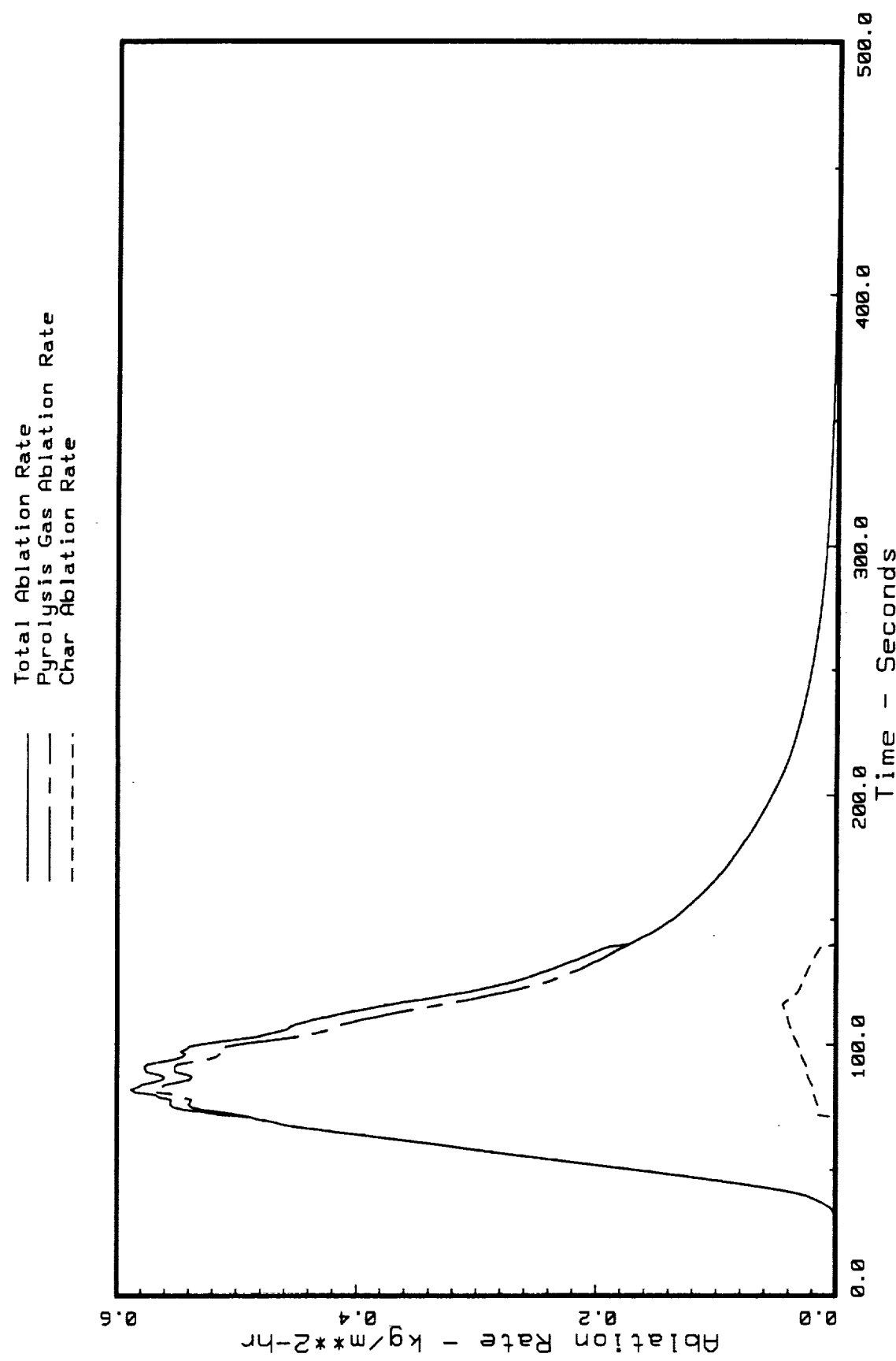


Fig. 24 Mars Aerocapture for the 12.192m AFE - Predicted Ablation Rate at the Stagnation Point

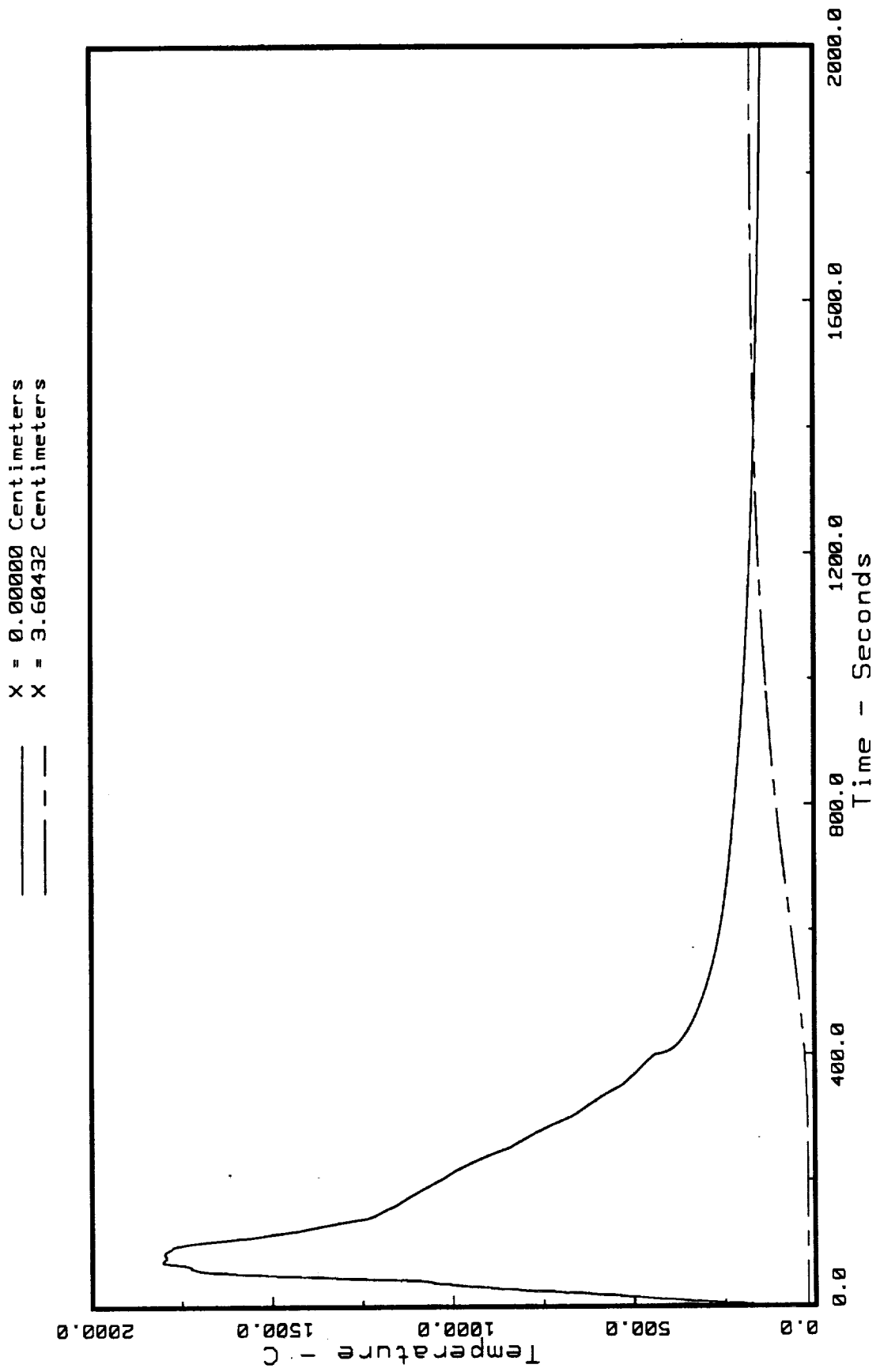


Fig. 25 Earth Aerocapture for the 12.192m AFE - Temperature Time History of the Ablator Surface and Graphite Epoxy Backwall for the First 2000 Seconds at the Stagnation Point

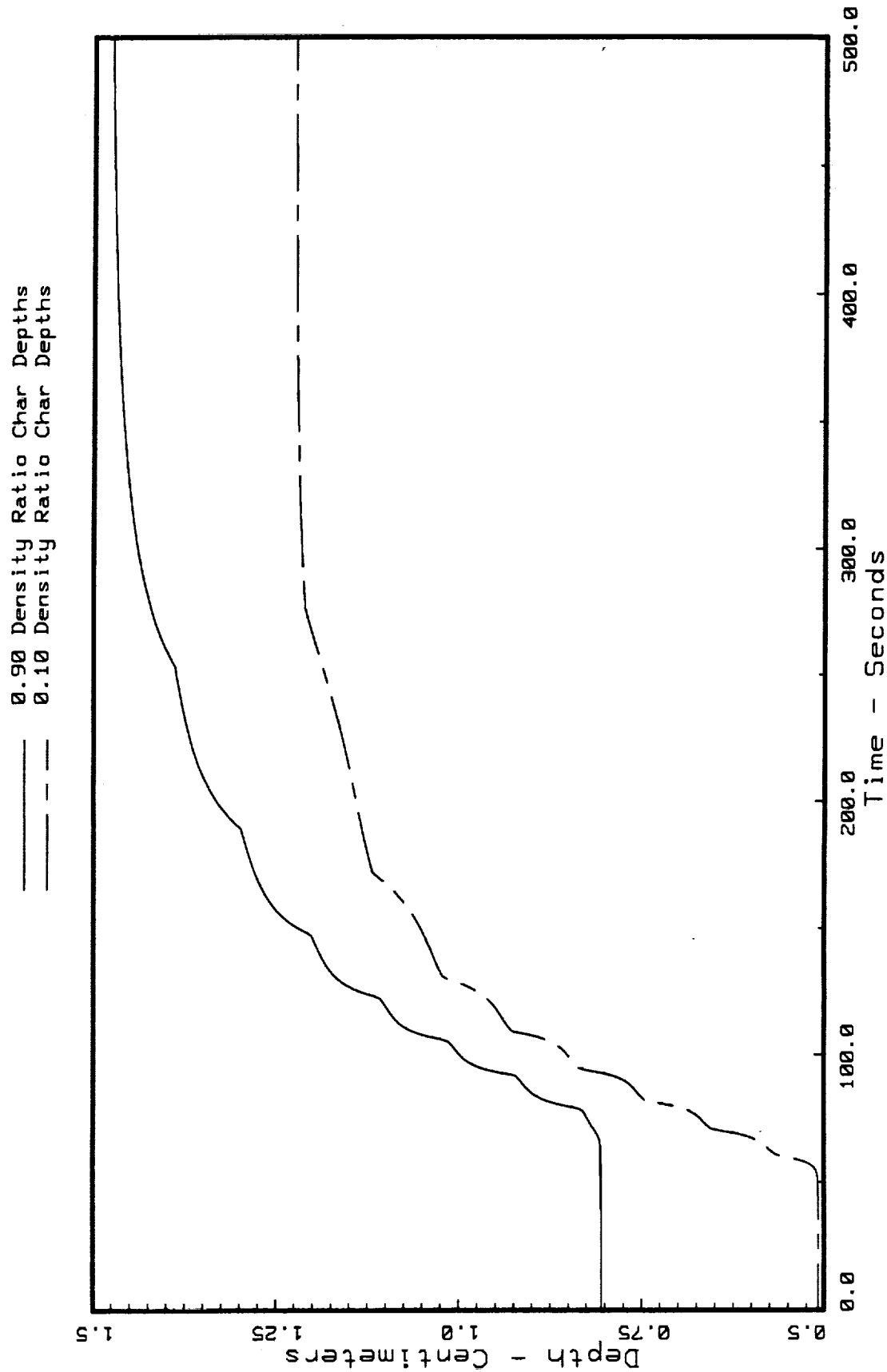


Fig. 26 Earth Aerocapture for the 12.192m AFE - 0.9 and 0.1 Char Density Ratio Depths
at the Stagnation Point

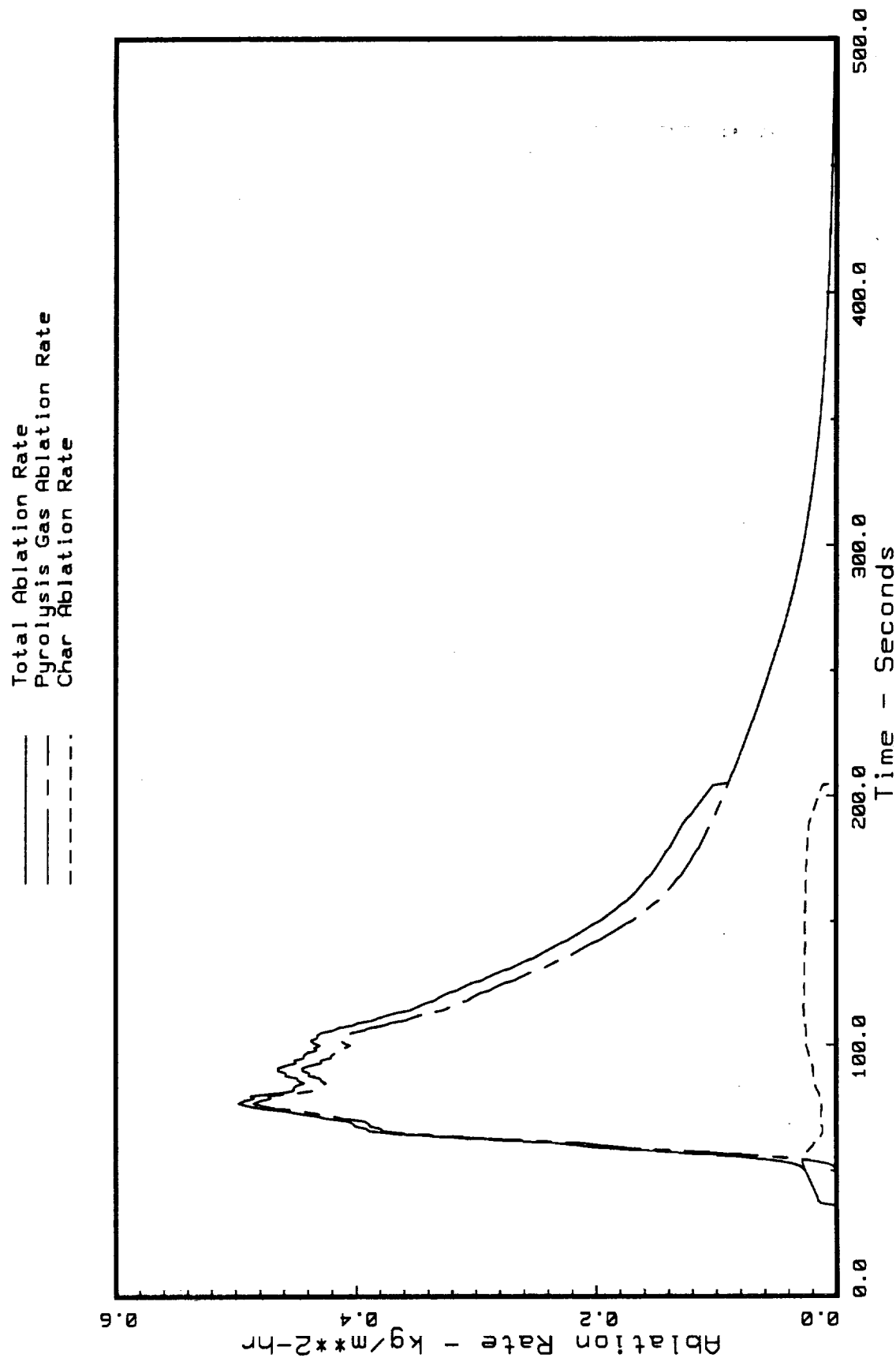


Fig. 27 Earth Aerocapture for the 12.192m AFE - Predicted Ablation Rate at the Stagnation Point

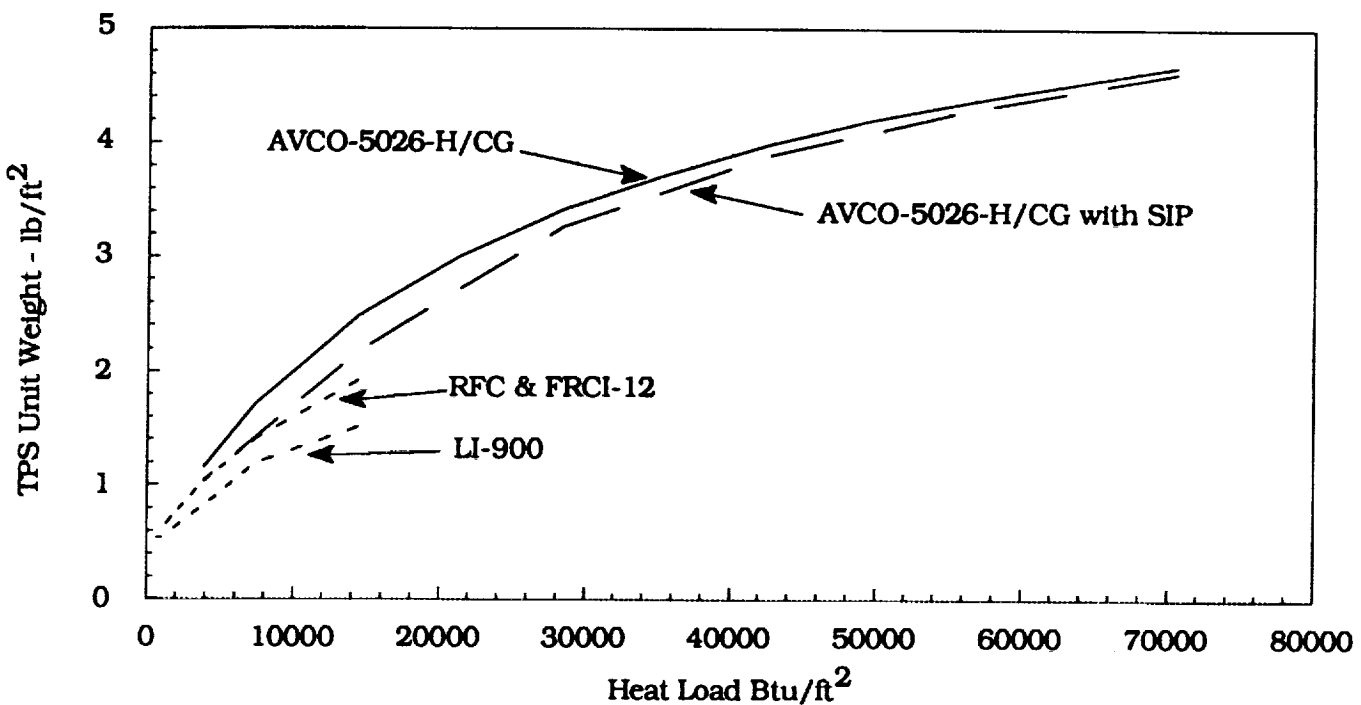


Fig. 28 TPS Unit Weight vs. Heat Load for a Vehicle ($0.61 \text{ m } R_N$ Biconic Entering at 12 km/s) Aerocapturing at Mars.

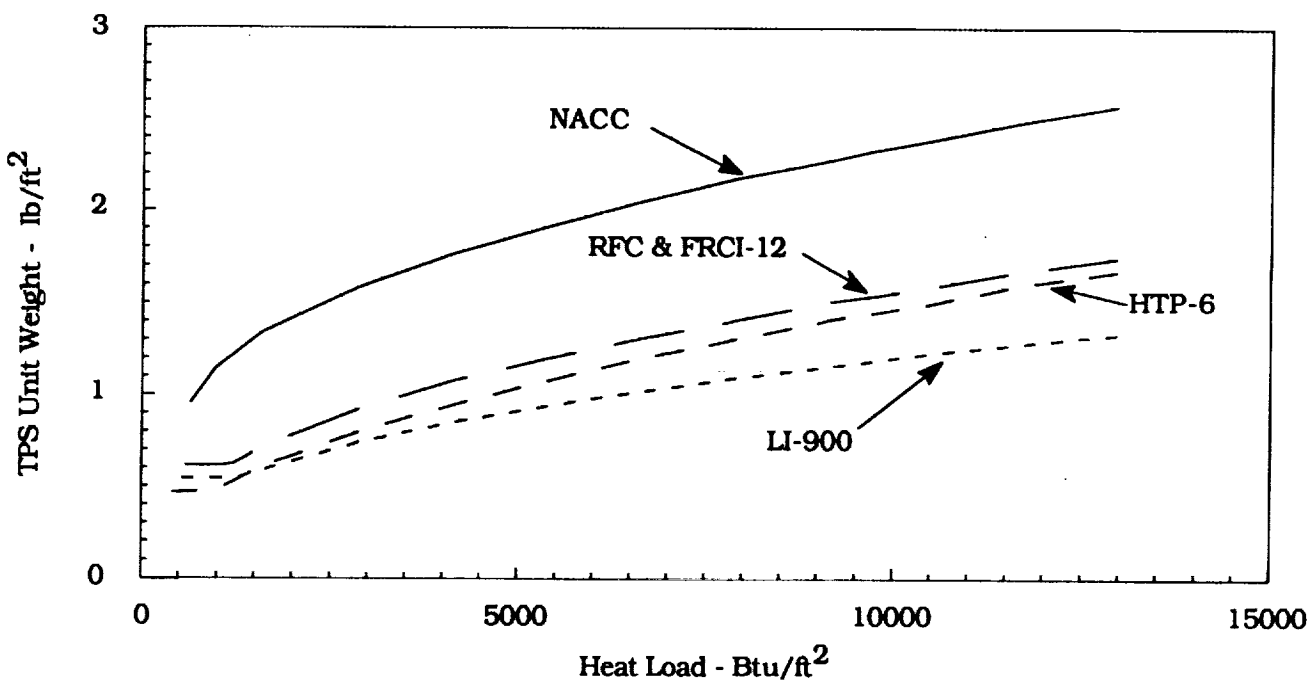


Fig. 29 TPS Unit Weight vs. Heat Load for a Vehicle (40° Domed Cylinder) Aerocapturing at Earth.

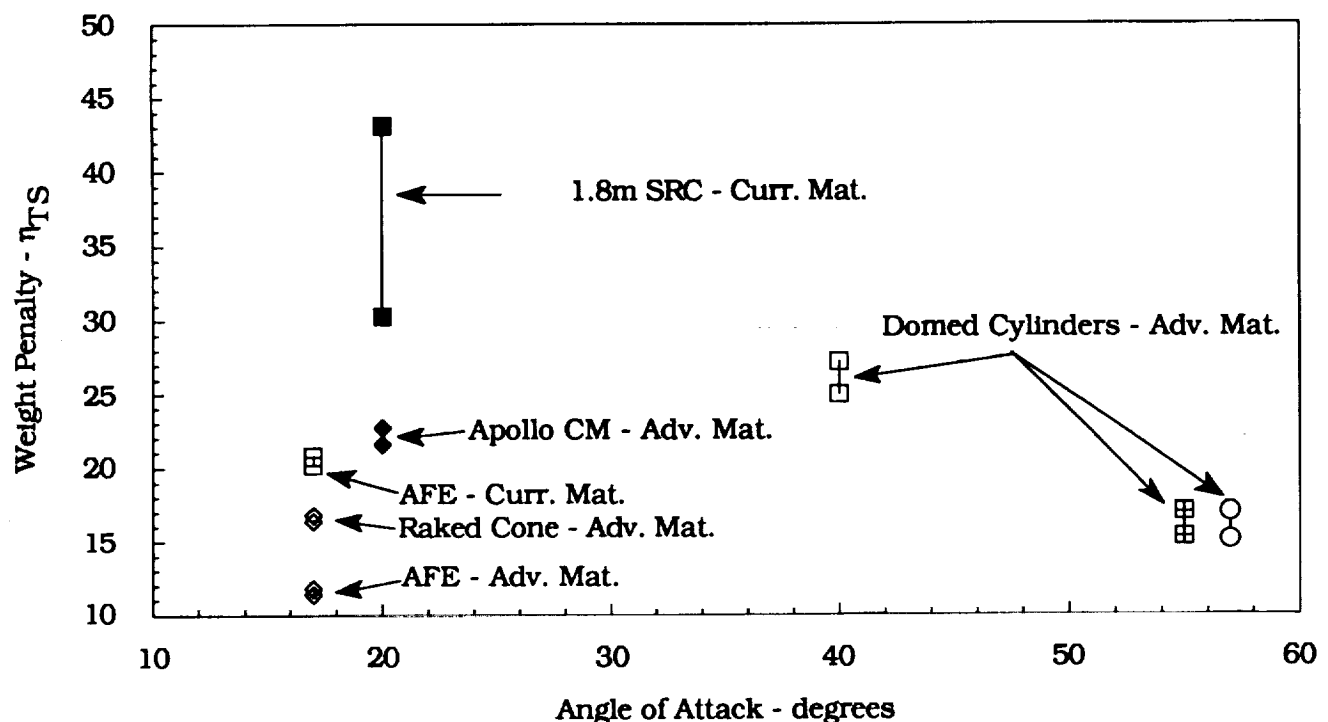


Fig. 30 Weight Penalty as a Function of Angle of Attack for Vehicles Aerocapturing at Earth.

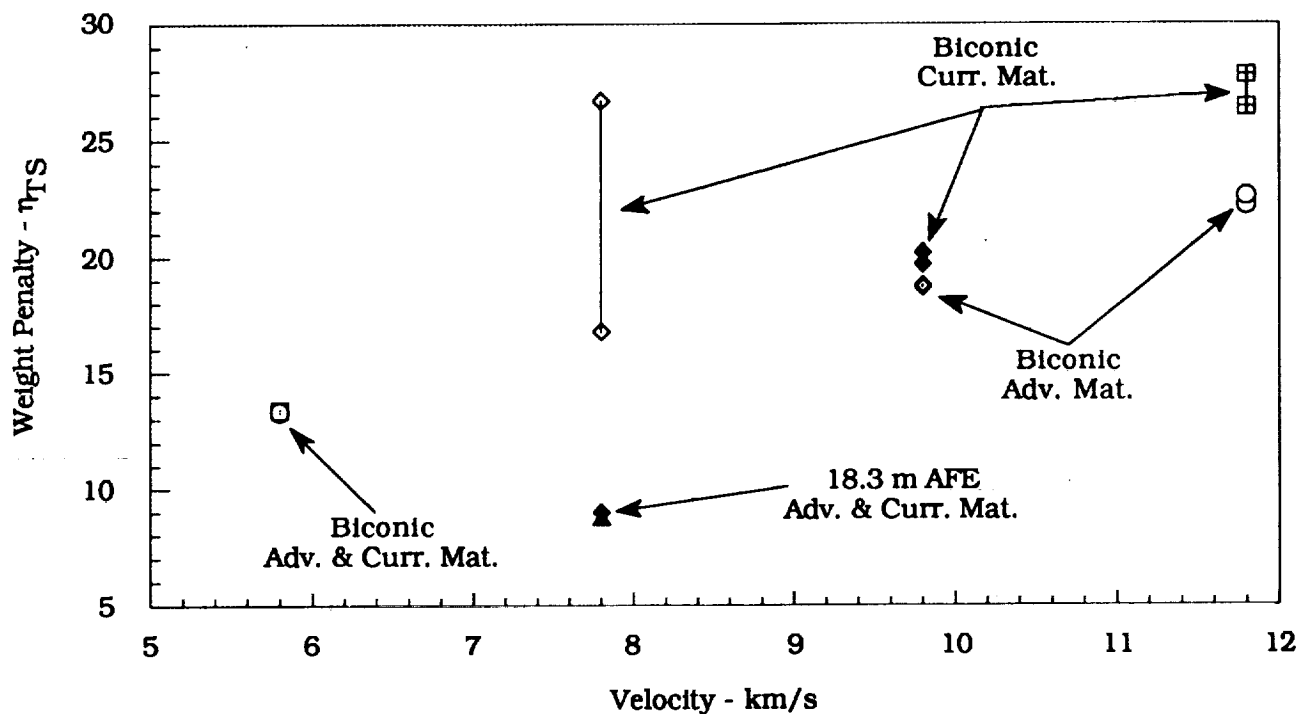


Fig. 31 Weight Penalty as a Function of Velocity for Vehicles Aerobraking at Mars.

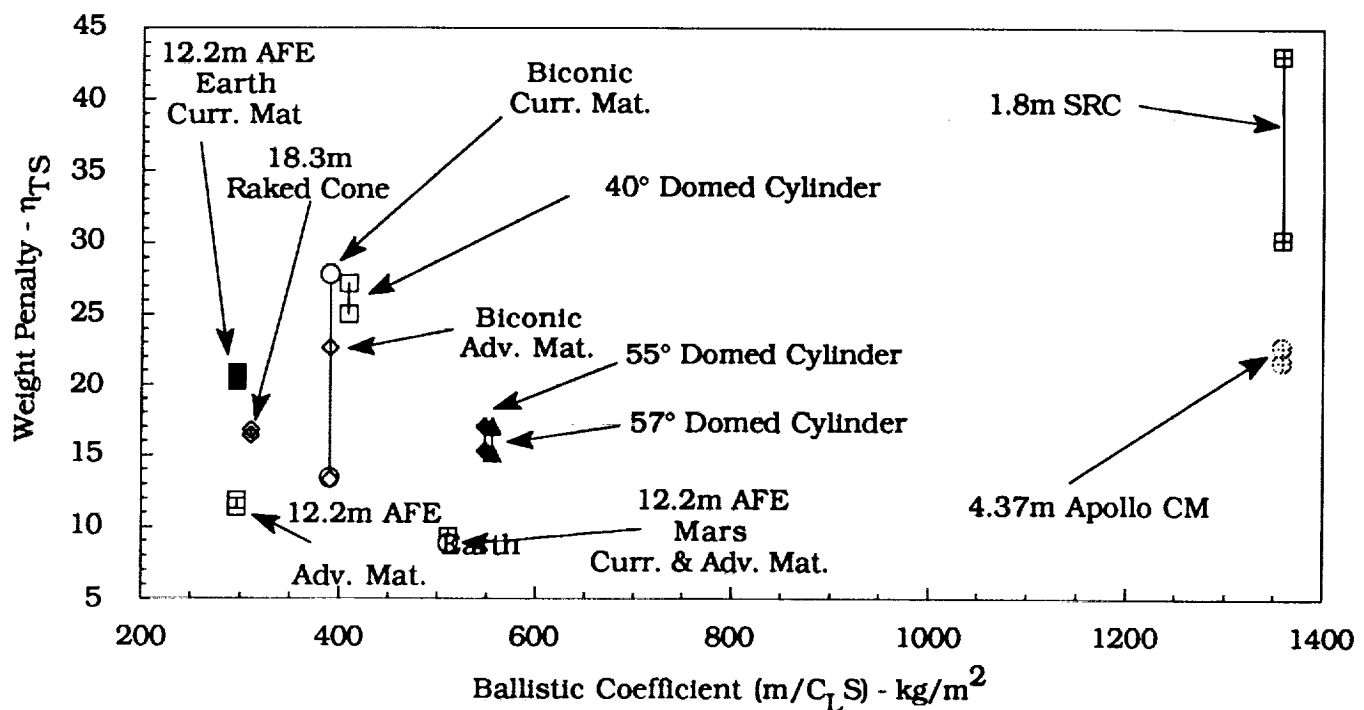


Fig. 32 TPS Weight Penalty vs. Ballistic Coefficient for All Vehicles.

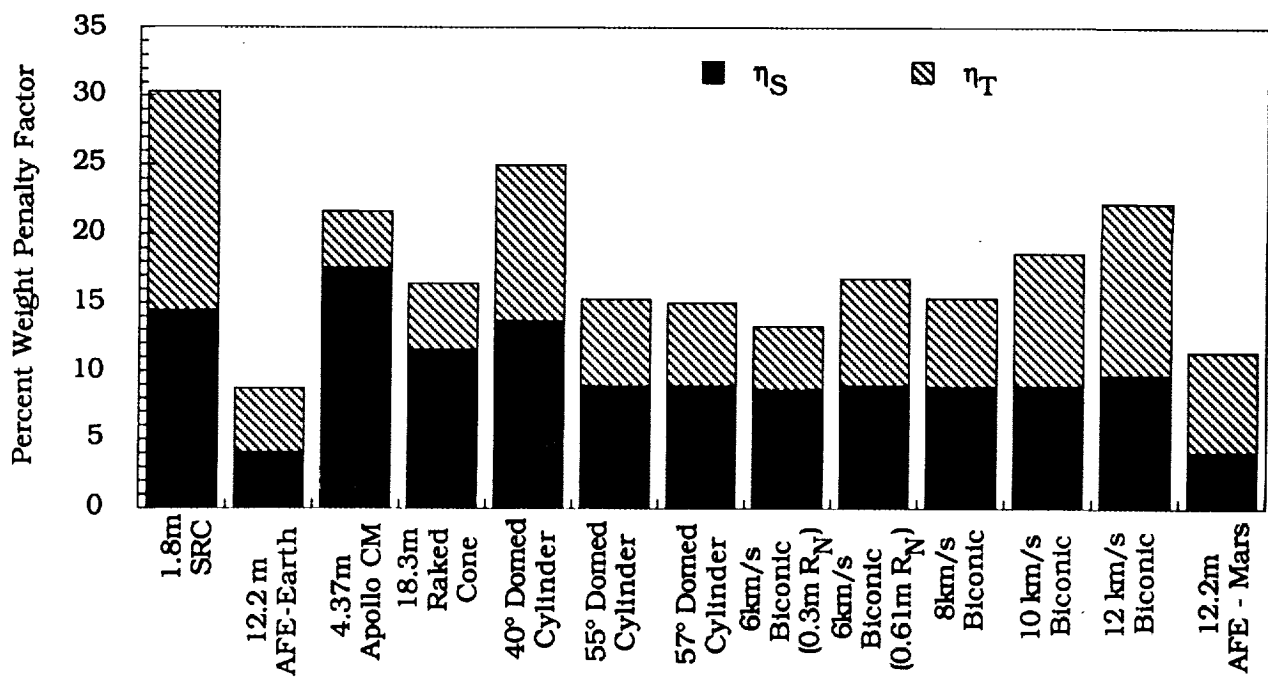


Fig. 33 Weight Penalty Factors for Best TPS/Structure Weights.

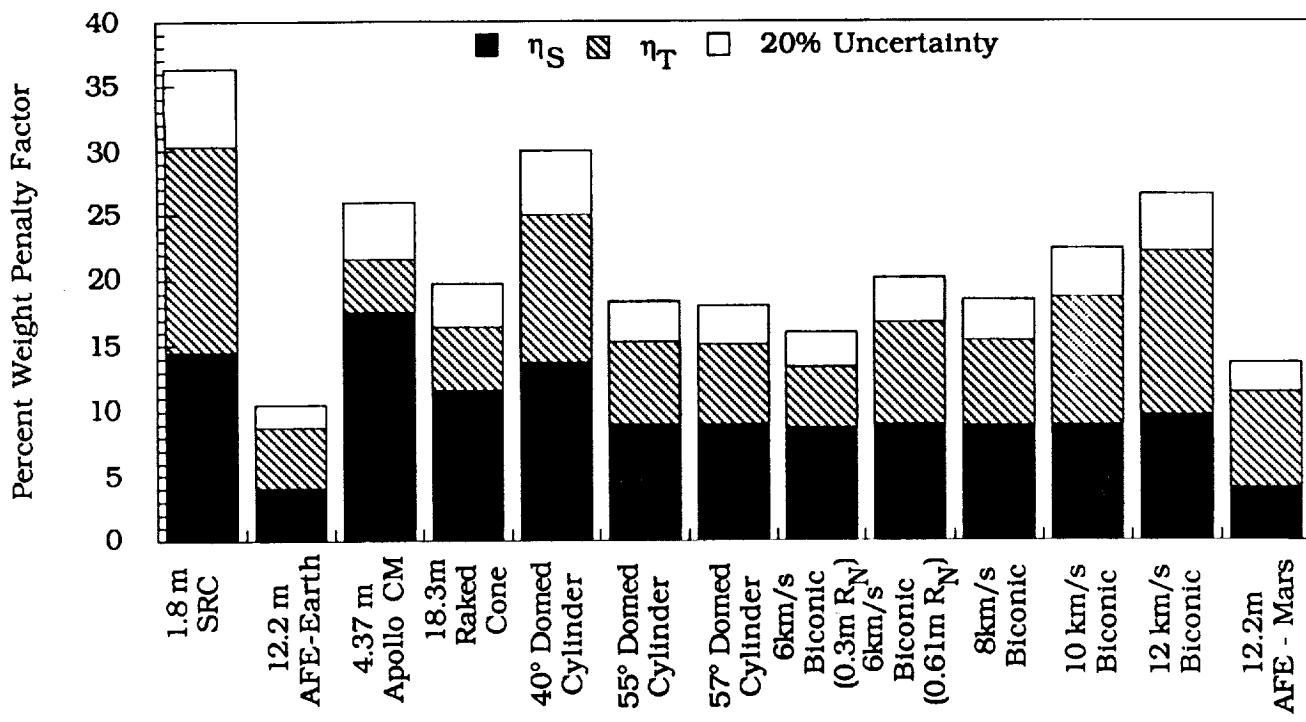


Fig. 34 Weight Penalty Factors for Best TPS/Structure Weights with 20% Uncertainty.

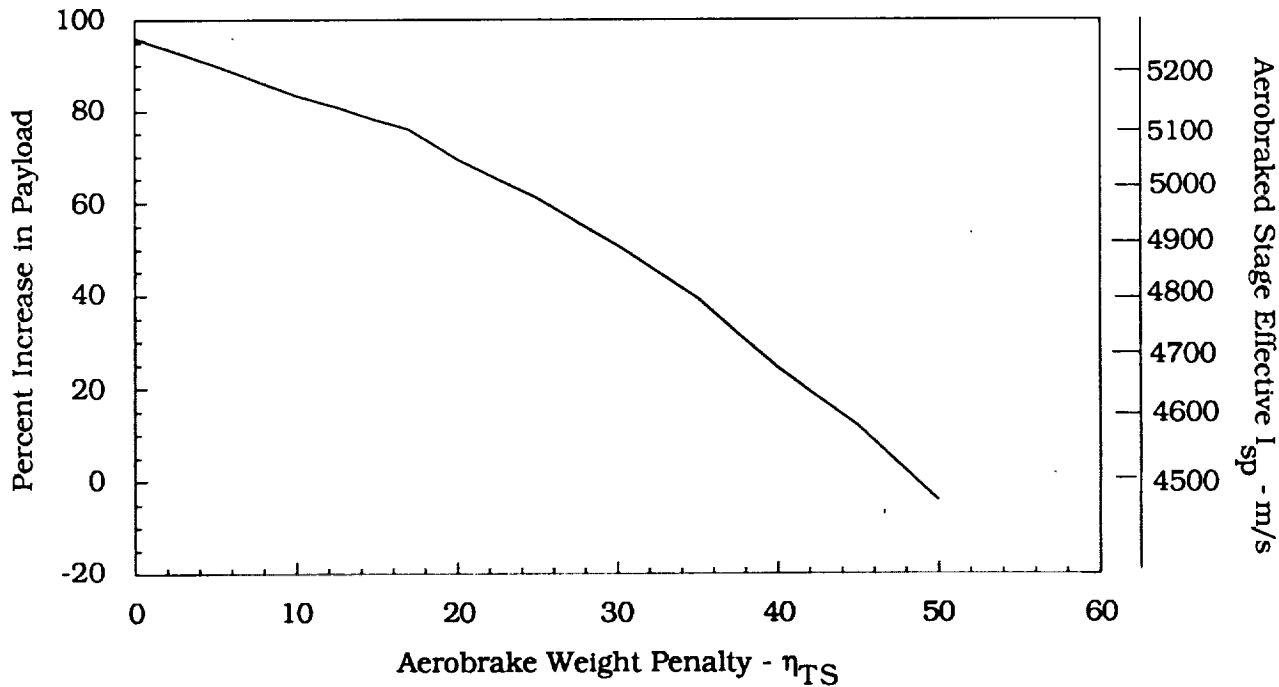


Fig. 35 Percent Increase of GEO Delivery Mass for Aerobraked Stage Over an All-Propulsive Stage.

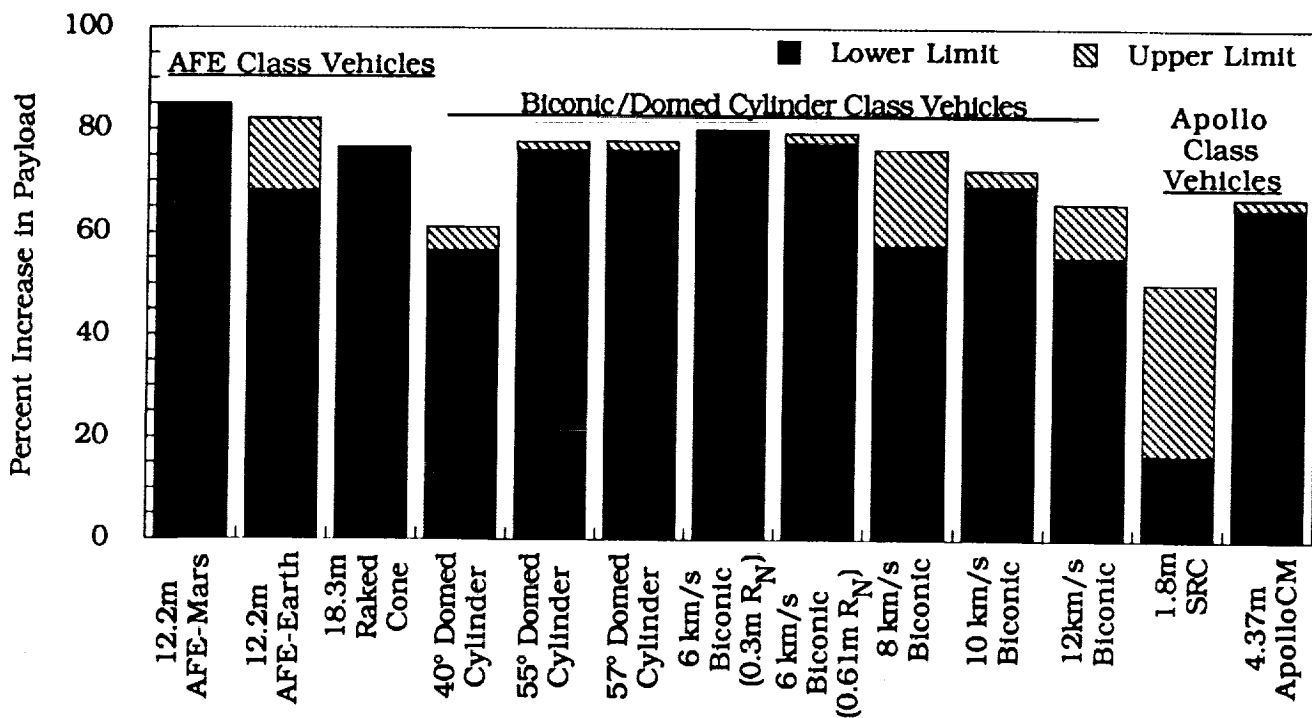
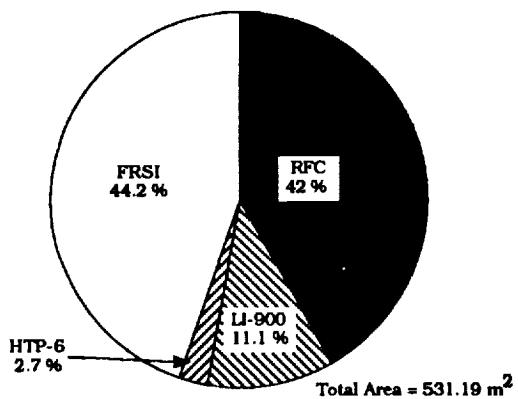
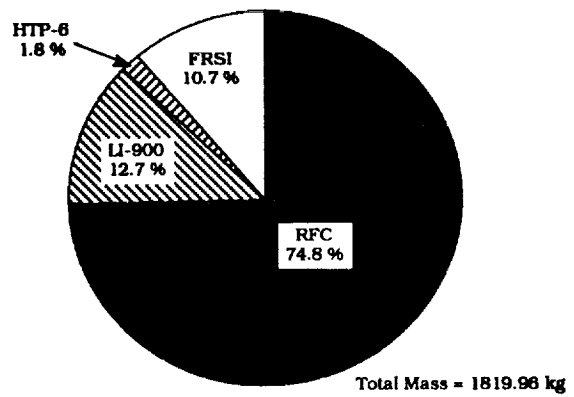


Fig. 36 Percent Increase in Payload Benefits for Aerobraking.



**Fig. 37 Relative Areas for the 57° Domed Cylinder
TPS - Advanced Material Technology.**



**Fig. 38 Relative Mass for the 57° Domed Cylinder
TPS - Advanced Material Technology.**

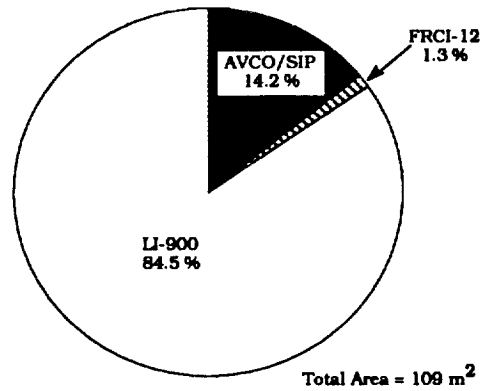


**Fig. 39 Relative Areas for the 10 km/s Biconic
TPS - Current Material Technology.**

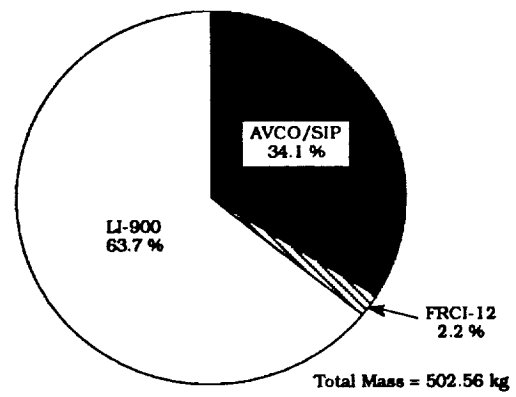


**Fig. 40 Relative Mass for the 10 km/s Biconic
TPS - Current Material Technology.**

REPORT DOCUMENTATION PAGE

*Form Approved
OMB No. 0704-0188*

Public reporting burden for this collection of information is estimated to average 1 hour per response, including the time for reviewing instructions, searching existing data sources, gathering and maintaining the data needed, and completing and reviewing the collection of information. Send comments regarding this burden estimate or any other aspect of this collection of information, including suggestions for reducing this burden, to Washington Headquarters Services, Directorate for Information Operations and Reports, 1215 Jefferson Davis Highway, Suite 1204, Arlington, VA 22202-4302, and to the Office of Management and Budget, Paperwork Reduction Project (0704-0188), Washington, DC 20503.

1. AGENCY USE ONLY (Leave blank)			2. REPORT DATE August 1991		3. REPORT TYPE AND DATES COVERED Technical Memorandum		
4. TITLE AND SUBTITLE TPS Design for Aerobraking at Earth and Mars					5. FUNDING NUMBERS		
6. AUTHOR(S) S. D. Williams (LESC), M. M. Gietzel (LESC), W. C. Rochelle (LESC), D. M. Curry (JSC)							
7. PERFORMING ORGANIZATION NAME(S) AND ADDRESS(ES) Structures and Mechanics Division NASA Johnson Space Center Houston, Texas 77058					8. PERFORMING ORGANIZATION REPORT NUMBER S-645		
9. SPONSORING / MONITORING AGENCY NAME(S) AND ADDRESS(ES) NASA Washington, D.C. 20546-001					10. SPONSORING / MONITORING AGENCY REPORT NUMBER NASA TM 104739		
11. SUPPLEMENTARY NOTES							
12a. DISTRIBUTION / AVAILABILITY STATEMENT Unclassified/Unlimited Subject Category 77				12b. DISTRIBUTION CODE			
13. ABSTRACT (Maximum 200 words) An investigation was made to determine the feasibility of using an aerobrake system for manned and unmanned missions to Mars, and to Earth from Mars and lunar orbits. A preliminary Thermal Protection System (TPS) is examined for five unmanned small nose radius, straight biconic vehicles and a scaled up Aeroassisted Flight Experiment (AFE) vehicle aerocapturing at Mars. Analysis is also presented for the aerocapturing into Earth orbit. Also analyzed were three different classes of Lunar Transfer Vehicles (LTVs): an expendable scaled up modified Apollo Command Module (CM), a raked cone (modified AFE), and three large nose radius domed cylinders. The LTVs would be used to transport personnel and supplies between Earth and the moon in order to establish a manned base on the lunar surface. The TPS for all vehicles analyzed is shown to have an advantage over an all propulsive velocity reduction for orbit insertion.							
14. SUBJECT TERMS Thermal Protection Systems, Aerothermodynamics, entry, Earth, Mars					15. NUMBER OF PAGES		
					16. PRICE CODE		
17. SECURITY CLASSIFICATION OF REPORT Unclassified		18. SECURITY CLASSIFICATION OF THIS PAGE Unclassified		19. SECURITY CLASSIFICATION OF ABSTRACT Unclassified		20. LIMITATION OF ABSTRACT UL	

